

AD No. 19 236
ASTIA FILE COPY

Office of Naval Research

Contract N50RI-76 • Task Order No.1 • NR-078-011

ON THE NUCLEAR MAGNETIC RESONANCE
IN METALS AND ALLOYS



By
N. Bloembergen
and
T. J. Rowland

August 20, 1953

Technical Report No. 186

Cruft Laboratory
Harvard University
Cambridge, Massachusetts

TR186

Office of Naval Research

Contract N5ori-76

Task Order No. 1

NR-078-011

Technical Report

on

On the Nuclear Magnetic Resonance in Metals and Alloys

by

N. Bloembergen and T. J. Rowland

August 20, 1953

The research reported in this document was made possible through support extended Cruft Laboratory, Harvard University, jointly by the Navy Department (Office of Naval Research), the Signal Corps of the U. S. Army, and the U. S. Air Force, under ONR Contract N5ori-76, T. O. 1.

Technical Report No. 186

Cruft Laboratory

Harvard University

Cambridge, Massachusetts

To be published in Acta Metallurgica, January 1953.

On the Nuclear Magnetic Resonance in Metals and Alloys

by

N. Bloembergen and T. J. Rowland

Division of Applied Science, Harvard University

Cambridge, Massachusetts

Abstract

The shift of the nuclear resonance and the line width has been measured in α - and β -tin, thallium, lead and several alloys. While gray tin has no shift relative to the resonance in insulating compounds, white tin has an anisotropic shift of 0.79 per cent along the tetragonal axis and 0.74 per cent perpendicular to it. A theory for the anisotropy and asymmetry of the observed line is given.

Thallium has an anomalously broad resonance line with a shift of 1.54 per cent. In thallium alloys the shift varies continuously with composition in each phase and has discontinuities when phase transitions occur. A maximum shift of 2.1 per cent has been found in a Tl Mg - alloy, while the Na Tl structure exhibits a negative shift of -1.0 per cent.

Quadrupolar effects are important, when the nuclear spin $I > \frac{1}{2}$. The intensity of the copper resonance in pure copper can be increased by annealing and decreased by cold work. In alloys like α -brass and copper-silver the intensity decreases rapidly with increasing zinc or silver content. At 25 per cent zinc, the copper resonance becomes unobservable. These effects are explained in terms of quadrupole interaction and can give information about the state of order or disorder on an atomic scale in the alloy.

1. Introduction

Nuclear magnetic resonance experiments have already yielded some interesting information on the electronic structure and self-diffusion in metals. The three main sources of information of nuclear resonance about the structure of matter are the position of the resonance line, the width and shape, and the spin-lattice relaxation time.

It was discovered by Knight¹ that the resonance frequency in metals is higher than for nuclei of the same isotope in an insulating material in the same magnetic field. The effect is caused by the local field produced by the conduction electrons as was first shown by Townes.² The internal field

produced at the position of the nuclei is much larger than might be anticipated from the electronic paramagnetic susceptibility, because of the partial S-wave character of the wave function. Let the expectation value for an electron with a wave vector \underline{k} near the Fermi level, to be at the nucleus in the metal, be given by

$$|\psi_{k \text{ met}}(0)|^2 = C_k |\psi_{\text{atom}}(0)|^2 \quad (1)$$

Here ψ_{met} is the metallic wave function normalized to unity over one atomic volume V_0 , $\psi_{\text{atom}}(0)$ is the atomic wave function where the conduction electron is supposed to be in an S-state outside a closed shell. The hyperfine interaction in the free atom in an S-state³ is given by

$$A \underline{I} \cdot \underline{S}$$

where the hyperfine structure constant is proportional to $|\psi_{\text{atom}}(0)|^2$. In the metal only $2\beta H_0 V_0 N(E_F)$ conduction electrons per atom have unbalanced spins, with magnetic moments parallel to H_0 . Here $\beta = \mu_{\text{el}}$ is the Bohr magneton and $N(E_F)$ is the density of states, the number of states per unit volume and per unit energy interval, at the Fermi level. For a free electron gas

$$V_0 N(E) = \frac{3}{4} E_F^{-1}$$

In the metal the nuclear spin and the electron spin will always be decoupled due to the strong interaction between conduction electrons. For a nuclear spin transition $\Delta m_I = \pm 1$, the interaction energy with the electron spins changes by an amount

$$\gamma \hbar \Delta H = \hbar \Delta \nu = \beta H_0 V_0 N(E) C A \quad (2)$$

Here C is a suitable average of C_k over the Fermi surface, γ is the nuclear gyromagnetic ratio, $\gamma \hbar I = \mu_N$ is the maximum value of the z-component of the nuclear magnetic moment. The relative Knight shift can thus be written in the form

$$\frac{\Delta H}{H_0} = \frac{\Delta \nu}{\nu_0} = \frac{\beta I}{\mu_N} C A V_0 N(E) \quad (3)$$

If $N(E)$ is known from electronic specific heat or magnetic susceptibility measurements, the value of C can be determined experimentally from the observed Knight shift and compared with theoretical values. One would expect the values of C to be of the order of unity, as the metallic wave function near the Fermi level will usually still have a large percentage of S-wave character and the renormalization factor should not change the order of magnitude.⁴ The observed values of $\Delta H/H_0$ are in agreement with the expectation and range from 0.026 per cent for Li to 1.54 per cent for thallium, the largest value reported so far for any element. This is, of course, directly related with the large value of atomic hyperfine splitting for this heavy element.

The relaxation time in metals has been discussed theoretically by Heitler and Teller,⁵ Korringa⁶ and Overhauser,⁷ and has been studied experimentally by Bloembergen,⁸ Poulis⁹ and Rollin.¹⁰ It is determined by the off-diagonal components of the nuclear spin-electron spin interaction. In the fundamental process these spins flip simultaneously $\Delta m_I = -\Delta m_S = \pm 1$. The balance of energy $\pm \hbar(\gamma_{el} - \gamma_n)H_0$ is taken up by a change in wave number of the conduction electron. Only electrons near the Fermi level can take up such a small amount of energy. The probability for the process is therefore proportional to kT and the complete theoretical expression for the relaxation time T_1 is

$$\frac{1}{T_1} = \frac{\pi kT}{\hbar} V_0^2 N^2(E) C^2 A^2 \quad (4)$$

From eqs. (3) and (4) follows Korringa's relation between the line shift and the relaxation time

$$T_1 \left(\frac{\Delta H}{H} \right)^2 = \frac{\hbar}{\pi kT} \left(\frac{\beta I}{\mu_N} \right)^2 \quad (5)$$

The relation eq. (5) is only approximately fulfilled. Another term should be added to the right-hand side of eq. (4) describing the interaction of the nuclear spin with the non-spherically symmetrical part of the electronic motion. The complete Hamiltonian for the nuclear spin interaction with the conduction electrons is

$$\mathcal{H} = \frac{8\pi}{3} \beta \gamma_N \hbar \mathbf{I} \cdot \mathbf{S}(\mathbf{r}) \delta(\mathbf{r}) - \beta \gamma_N \hbar \mathbf{I} \cdot \left(\frac{\mathbf{S}}{r^3} - \frac{3}{r^5} \mathbf{r}(\mathbf{S} \cdot \mathbf{r}) \right) \\ - \gamma_N \hbar \frac{e}{mc} \left(\mathbf{S} \cdot \frac{[\mathbf{r} \times \mathbf{p}]}{r^3} \right) + \frac{e^2 Q}{r^3} \left(3 \mathbf{I} \cdot \mathbf{I} - \epsilon \mathbf{I}^2 \right) \cdot \left(3 \mathbf{r} \cdot \mathbf{r} - \epsilon \mathbf{r}^2 \right) \quad (6)$$

Here \mathbf{r} is the radius vector of the electron with the nucleus at the origin.

The first term is the point interaction discussed before. The second term represents the interaction of the nuclear spin with the electron spin, the third term with the electron orbit, the last term is the quadrupole interaction, not included in Korringa's paper. To find the matrix elements the terms of the Hamiltonian must be integrated over the multi-electron wave function of the metal. In our approximation we integrate over a one-electron wave function $\psi_{\mathbf{k}}$ and then sum over all wave numbers \mathbf{k} . The orbital angular momentum \mathbf{p} in the metal is quenched. There is no preference for a left- or right-handed motion of the electrons, and this interaction will not contribute to the Knight shift in a first approximation. The spin-spin interaction, the second term on the right side of eq. (6), will make a contribution in a non-cubic crystal. The effect will depend on the angle of the crystalline axes and the external field, and the average for a polycrystalline specimen will be zero. This anisotropy of the Knight shift will be discussed in detail in section 5 below. It leads to a spurious broadening and asymmetry of the line in polycrystalline material, which is proportional to the external magnetic field. If the crystal is non-cubic and if the nuclear spin $I \geq 1$, the last term does not vanish. In polycrystalline material the quadrupole interaction will give rise to a broadening of the line which will be discussed more fully in section 2. Clearly the complete quadrupole interaction also includes the effect of nuclear charges and non-conduction electrons. All these contributions to the inhomogeneous electric field can be lumped together in discussing the line position and broadening.

The contribution of the Hamiltonian eq. (6) to the relaxation time has a different character. For the Bloch-type one-electron wave functions $\phi_{\mathbf{k}}$ and $\phi_{\mathbf{k}'}$, non-diagonal elements of the type $\mathcal{H}_{\mathbf{k}\mathbf{k}'}$, must be squared, averaged over the Fermi distribution and multiplied by the density of final states to obtain the total transition probability. The contribution of the

last three terms is now nonvanishing even in cubic crystals, since the individual wave function ϕ_k does not have this symmetry. This result has to be added to the right-hand side of eq. (4), and the relaxation time should be shorter than that calculated from eq. (5). This has been found generally to be the case.¹¹ Since only electrons near the tail of the Fermi distribution will be able to take up the small amount of energy of the processes involved, the transition probability will remain proportional to the absolute temperature and independent of the external field, even if the complete Hamiltonian is used. The Korringa relation should be more closely obeyed, the more dominant the S-wave character of the one-electron wave functions near the Fermi level.

The inverse proportionality between T_1 and T has been established rather satisfactorily in a number of cases, although a notable exception is presented by Cesium at high temperatures.¹¹ There is no confirmation that T_1 is independent of H_0 . In fact, a few results by Poulis indicate otherwise. More data on the H_0 -dependence of T_1 are desirable. Deviations from the theoretical behavior eqs. (4) and (5) could be attributed to correlation and exchange effects, omitted in the one-electron approximation. It is not clear how the effective density of "one-electron states" could depend very strongly on H or T , even if the interaction between electrons is taken into account.

The experimentally observed shifts ΔH are indeed proportional to H and seem to be independent of T , except for a small and rather trivial volume effect.

The line-width is determined by the nuclear dipolar interaction and by the finite life-time T_1 caused by the relaxation mechanism. The second moment of the absorption line due to dipolar interaction in a polycrystalline powder is given by

$$\frac{1}{\gamma^2 T_2^2} = \left\{ (\Delta H^2)_{Av} \right\} = \frac{3}{5} I(I+1) \gamma^2 \hbar^2 \sum_j r_{oj}^{-6} + \frac{4}{15} \sum_f I_f(I_f+1) \gamma_f^2 \hbar^2 r_{of}^{-6} \quad (7)$$

The summation j extends over identical nuclei in the crystal, the summation f includes all different nuclei. Gutowski¹¹ has shown that in metals at higher

temperatures the contribution of the relaxation mechanism to the width amounting to $(1/2 T_1)$ is important. In that case the width will increase proportionally with the temperature. The relaxation mechanism will nearly always be the width-determining factor above the melting point. In the liquid state the dipolar interaction of the nuclei has to be averaged over the Brownian motion and is reduced to a very small value. A decrease in the dipolar width has been observed with increasing temperature in the solid metals lithium and sodium, when the self-diffusion becomes sufficiently rapid.^{11, 12, 13} This phenomenon is entirely analogous to the motional narrowing occurring in liquids and could be expected to occur in other metals just below the melting point. It gives information about the self-diffusion as a function of temperature when the elementary jumping process of the diffusion has a frequency larger than T_2^{*-1} .

It seems profitable to extend the observations of the shift, width and relaxation time to alloys, in order to gather information about the density of states and electronic structure in these systems. In the next section we shall discuss the importance of quadrupole interaction in alloy systems and the difficulties presented by it.

The equipment consisted of a Pound-Knight-Watkins type of radiofrequency spectrometer^{14, 15} and a permanent magnet with a field near 6000 gauss in a $1\frac{1}{4}$ -inch gap, the diameter of the pole faces being 4 inches. The field was calibrated by the proton or Li^7 resonance in an aqueous solution of LiCl . The inhomogeneity in the volume occupied by the samples was less than 0.4 gauss, or negligible compared to the width of most resonances described in this paper. The field in the gap was found to vary with temperature, about -1.3 gauss per $^\circ\text{C}$, probably due to the expansion of the magnet yoke. The temperature of the magnet was always recorded and a correction to the magnetic field was applied. A few measurements were made at fields between 2000 and 5500 gauss with an electromagnet. This magnetic field was less homogeneous and drifted with time. Further measurements at other field strengths will be carried out with an improved electromagnet. The frequency of the oscillator was compared with the frequency of a standard frequency meter with an estimated error of less than 100 cps.

The magnetic field was modulated sinusoidally at 280 cps with amplitudes ranging between 0.2 and 20 gauss. To detect the weak broad lines the larger modulation amplitudes are necessary. The frequency of the oscillator was slowly swept through the resonance and its output fed into a phase-sensitive detector with a time constant of 8 sec (effective band-width about $\frac{1}{8}$ cps). The derivative of the absorption in the sample as a function of frequency was recorded on an Esterline-Angus recording instrument.

Due care should be taken that the experimentally observed quantities really correspond only to nuclear absorption. This will be true only when the metallic particle size is small compared to the skin depth.¹⁶ If this condition is not fulfilled, part of the observed signal may be due to eddy-current losses and corrections should be applied in order to evaluate the correct line shift and relaxation time. The metallic samples are always used in a finely divided polycrystalline form to increase the effective volume as the radiofrequency field cannot penetrate further than a few skin depths. Although experiments on single crystals would be desirable it would be difficult to make the effective volume of the sample sufficiently large.

The samples were made from powdered metals suspended in mineral oil. Oxygen-free electrolytic copper, thallium, lead, tin (c.p. grade), mercury (triply distilled), and zinc (s.p.) were obtained commercially. Alloys were made by melting weighed ratios of the constituents in an evacuated quartz or glass tube. They were allowed to cool slowly and were held at appropriate annealing temperatures to bring about equilibrium in the phases under consideration. The metals were then filed and sieved through a 200-mesh sieve. The particle size was smaller than the skin depth in all cases, and it could be assumed that the whole weight of the powdered sample contributed equally to the absorption signal. Insulation between the particles was achieved either by a very thin oxide coating or by the oil in which they were suspended. In some instances the powders were annealed in an inert atmosphere. In the oil suspension, particles could even be heated above their melting point without agglomeration. The glass tube containing the suspension was inserted in a shielded radiofrequency coil. The assembly could be inserted in a Dewar flask with a tail of 10-mm inside and 18-mm outside diameter for measurements at 77°K. In another assembly a heater

wire was wrapped around the shield of the coil. A thermal insulating layer on the outside made it a miniature oven. The temperature could be raised to 350°C. The modulation coils were outside the Dewar or oven. The coil was connected to the oscillator by a coaxial cable 20 inches long.

2. Quadrupole Effects

When it was attempted to detect the magnetic resonance of the copper isotopes in brass (80% Cu and 20% Zn), the signal was unobservable, although a similar volume of pure copper gave a signal to noise ratio of over one hundred. This rather unexpected result can be explained by considering quadrupole interaction.¹⁷ Although the crystallographic structure of α -brass as determined by X-rays has cubic symmetry, the environment of individual copper nuclei in the solid solution will not have this symmetry. If a few of the nearest neighbors are Zn-atoms the cubic symmetry has certainly disappeared on a microscopic scale. There may then exist gradients of the electric field which will vary in direction and magnitude at the position of the various copper nuclei. If a copper atom happens to have twelve other copper atoms as nearest neighbors, there may still be a deviation from cubic symmetry arising from Zn atoms among the next nearest or further neighbors, although in this case the magnitude of the gradient can be expected to be smaller. Even in pure copper a certain inhomogeneity of the internal electric field will exist due to strains around dislocations or other imperfections in the lattice. It has been shown by Pound and Watkins^{15, 18} that these strains in single crystals of the alkali halides are sufficient to wipe out the satellite transitions, i. e., the resonance of bromine and iodine nuclei in KBr and KI crystals is due solely to transitions between the levels with $m_I = \frac{1}{2}$ and $m_I = -\frac{1}{2}$. The reason is that the energy difference between these two levels is unaffected by the quadrupole interaction, as the first-order approximation quite generally depends on m_I^2 only. There is a first-order perturbation of the other energy differences, and these transitions are spread out over such a large frequency interval as to become unobservable. It is possible that in pure and well-annealed metals the quadrupole broadening is considerably less and that the satellite transitions also contribute to the signal. Evidence for this will be presented below. It is true that the metals

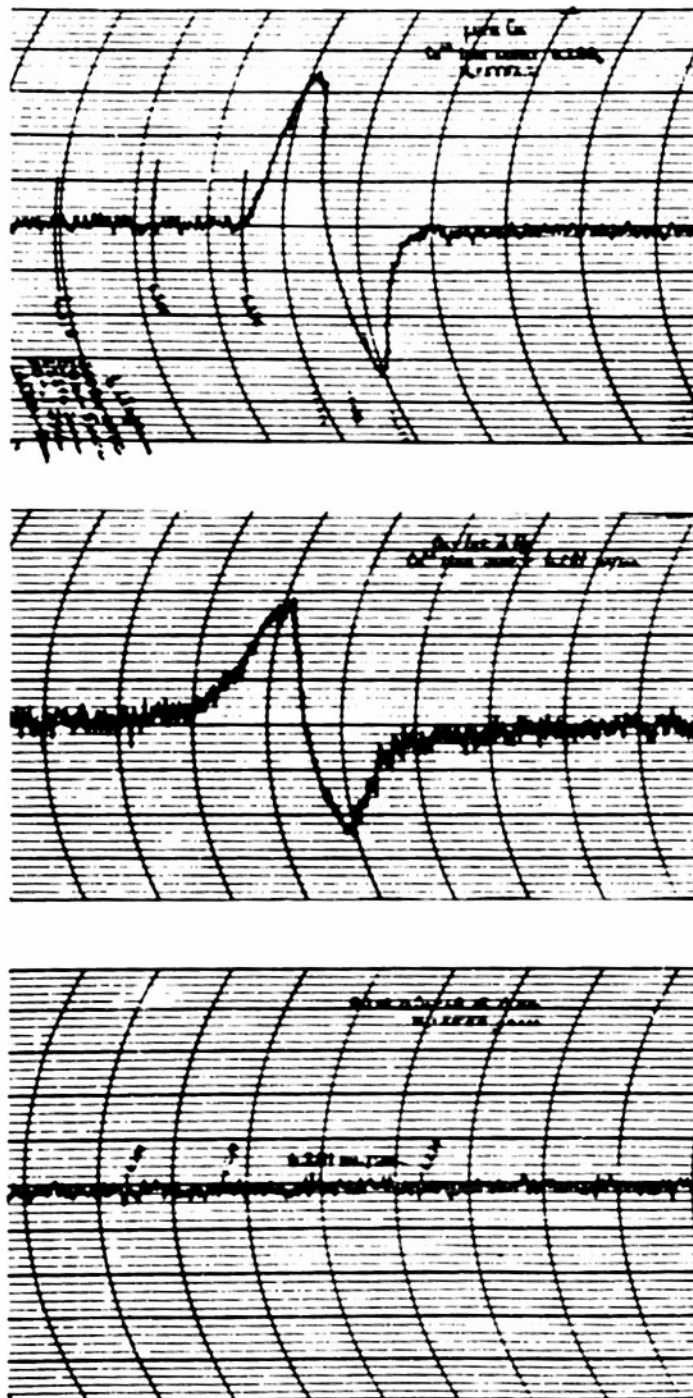


Figure 1. A recording of the derivative of the absorption of the Cu^{63} resonance at room temperature in upper: pure annealed copper; middle: 99% Cu and 1% Ag. [Note the appearance of weak tails, absent in pure copper.] lower: 80% Cu - 20% Zn. An extremely weak resonance with an intensity less than 1% of that in pure copper has been observed at 77°K in this alloy.

will have at least the same density of dislocations as the alkali halide crystals. But the electron orbits in the metal ions are probably deformed less under the influence of strains than of the Br^- and I^- ions. Furthermore, the quadrupole moments of the Cu isotopes are a factor 2 smaller than that of Br^{79} . Finally, the effect of strains in metals on the electric field gradient at a nucleus a few interatomic distances away will be smaller because atoms are displaced rather than positive or negative ions carrying a net charge.

The disappearance of the resonance line in alloys with a spin $I = \frac{3}{2}, \frac{5}{2}, \text{etc.}$, will then occur in two steps. At first the quadrupole interaction will wipe out all transitions except the $m = \frac{1}{2} \rightarrow -\frac{1}{2}$ transition by a first-order perturbation process. We shall write down the formulas for the case of axial symmetry of the inhomogeneous field. This will be correct if one solute atom is in particular responsible for the field. For somewhat higher solute concentrations in the solid solutions it is by no means correct. Nevertheless, the right order of magnitude of the line displacement and broadening will be obtained in this case. Let θ be the angle between the external magnetic field and the axial electric field. The first-order quadrupole perturbation gives for the frequency of the transition

$$\Delta W_{m \rightarrow m-1} = h \nu_0 - (2m-1)(1 - 3\cos^2\theta) \frac{3e^2 q Q}{8I(2I-1)} \quad (8)$$

It is seen that the frequency of the transition $m = \frac{1}{2} \rightarrow -\frac{1}{2}$ is not changed in this approximation. The satellite lines are broadened since all angles θ will occur in the polycrystalline sample. Summing over all angles we find that each satellite line has a second moment in a polycrystalline powder

$$\overline{(\Delta W)^2} = (2m-1)^2 \frac{9}{64} \frac{e^4 q^2 Q^2}{I^2 (2I-1)^2 h^2} \frac{4}{5} \quad (9)$$

On the average these lines are not displaced since $\overline{1 - 3\cos^2\theta}_{\text{Av}} = 0$. The line shape is quite characteristic and has been described in other papers. Often the broadening, of which eq. (9) gives the magnitude, will make the lines unobservable. The transition $m = \frac{1}{2} \rightarrow -\frac{1}{2}$ will only be broadened in

a second approximation according to the equation

$$\Delta W_{\frac{1}{2} \rightarrow -\frac{1}{2}} = h \nu_0 + A (1 - 9 \cos^2 \theta) (1 - \cos^2 \theta) \quad (10)$$

$$A = \frac{9}{64} \frac{2I + 3}{4I^2(2I - 1)} \frac{e^4 Q^2 q^2}{h \nu_0} \quad (11)$$

The center of gravity of the line will be displaced toward lower frequencies by an amount

$$\overline{\delta \nu} = A h^{-1} \int_0^{\pi/2} (1 - 9 \cos^2 \theta) (1 - \cos^2 \theta) \sin \theta d\theta = -\frac{8}{15} A h^{-1} \quad (12)$$

while the second moment of line averaged over all angles is

$$\overline{(\delta \nu + \frac{A}{h} \frac{8}{15})^2} = 0.93 A^2 h^{-2} \quad (13)$$

The experiment in brass (20% Zn) was carried out at a frequency $\nu_0 = 6.3$ Mc/s. The line should have been at least 50 kc wide in order to escape observation. This enables us to calculate a lower limit for q or grad E in the alloy. Substituting the values $^{19}Q^{63} = -0.157 \times 10^{-24} \text{ cm}^2$ (or $Q^{65} = -0.145 \times 10^{-24} \text{ cm}^2$) and $\Delta \nu = 50 \text{ kc}$ in eq. (9), we find that $\frac{e^2 Q q}{h} > 0.17 \times 10^6 \text{ cps}$ is necessary for the satellites to disappear. A more stringent requirement is obtained from eq. (13). The condition that the line $m = \frac{1}{2} \rightarrow -\frac{1}{2}$ disappear gives

$$\frac{e^2 Q q}{h} > 2.6 \times 10^6 \text{ cps}$$

or

$$q = 4.8 \times 10^{23} \text{ cm}^{-3}$$

The simplest picture one can form about the origin of the internal electric field is that the Zn atoms have a different charge. The bivalent

Zn atoms will produce one extra positive electronic charge at their lattice sites compared to the monovalent Cu atoms. The electrons around the Zn atom are redistributed around the Zn atom — either by the formation of a bound state or a distribution of conduction electrons — to produce a screened Coulomb potential of the form^{20,21}

$$V = \frac{e}{r} e^{-Kr} \quad (14)$$

where a reasonable value for $K = 10^8 \text{ cm}^{-1}$. Differentiating this expression twice, we obtain for the gradient

$$eq = \frac{\partial E}{\partial r} = \frac{2e}{r^3} e^{-Kr} \left(1 + Kr + \frac{1}{2} K^2 r^2 \right) \quad (15)$$

One Zn atom would produce a gradient at the nearest Cu atom ($r = 2.55 \times 10^{-8} \text{ cm}$) of $q = 6.4 \times 10^{22} \text{ cm}^{-3}$. This is much smaller than the experimental limiting value. The effect should, moreover, depend strongly on the effective valency of the alloying agent. Actually, it is observed that silver produces at least as large a quadrupole broadening as zinc. Although Huang²² has shown that considerable polarization effects may occur even if the solvent and solute atom have the same valency, a description in terms of distorted electron orbitals is more appropriate, as will be discussed below.

It is of interest to investigate how the apparent line intensity decreases as the concentration of Zn or Ag increases. In Figure 2 the maximum absorption, corrected for the effective number of copper nuclei in the sample, is plotted as a function of the solvent concentration 1 - C.

In pure copper samples the intensity varies between 0.4 and 1.0. The unit intensity was assigned to a well-annealed pure electrolytic copper sample. Cold-worked copper filings then had an intensity between 0.4 and 0.5 with respect to this reference point. The intensity could be increased by a factor of nearly two when the cold-worked powder was annealed. The strains connected with dislocations in the worked material produce electric field gradients which wipe out the transitions $m_1 = \frac{3}{2} \rightarrow \frac{1}{2}$ and $m_1 = -\frac{1}{2} \rightarrow -\frac{3}{2}$ by first-

order quadrupole perturbation. The intensity ratio of these satellites to the central line $m = \frac{1}{2} \rightarrow -\frac{1}{2}$ is 3:4:3. The remaining intensity of 0.4 is thus ascribed to the $m = \frac{1}{2} \rightarrow -\frac{1}{2}$ transition.

In the cold-worked powdered alloys the intensity then decreases further by second-order quadrupole perturbation of the central line. However, the line does not broaden gradually nor does it show a shift toward lower frequencies, as could be expected from eqs. (12) and (13). Only a vestige of a broadened tail is apparent in the recording for a Cu-Ag alloy. We assume, therefore, that the electric field gradient is very large and makes the line unobservable, when a Zn or Ag atom is very close to a copper atom, but is rather small and does not affect the central line, when the Zn or Ag atoms are further away. Let the Zn atom in n neighboring positions around a copper nucleus make its resonance unobservable, and let the effect of the Zn atom be zero, if it is not in one of these n positions. We calculate the probability that a copper atom has no Zn atom in its neighboring lattice sites. If the relative concentration of the solute is C , each lattice site in the random solute solution of α -brass has a probability $1-C$ to be occupied by a Cu atom. The desired probability is therefore $(1-C)^n$. In this case the copper atom is surrounded only by copper atoms. The immediate neighborhood has cubic symmetry and the copper nucleus will contribute to the resonance signal. There are, of course, a few other configurations with cubic symmetry (e.g., all neighbors are Zn atoms) but for low Zn concentrations these have a much smaller probability and need not be considered here. We therefore find for the apparent intensity

$$\ell n \mathcal{I} = n \ell n (1 - C) .$$

In Figure 3 we have plotted \mathcal{I} versus the composition on a double logarithmic scale. It is seen that the experimental points fall surprisingly well on a straight line. Its slope determines $n = 18$. If this number came out much larger our theory would be incorrect as the underlying assumption that was only relatively few neighbors produce an appreciable gradient. The face-centered cubic lattice of copper has 12 nearest neighbors at a distance of 2.55 \AA and six next nearest neighbors at a distance 3.61 \AA . The number of these positions agrees well with the experimental value. The quadrupole

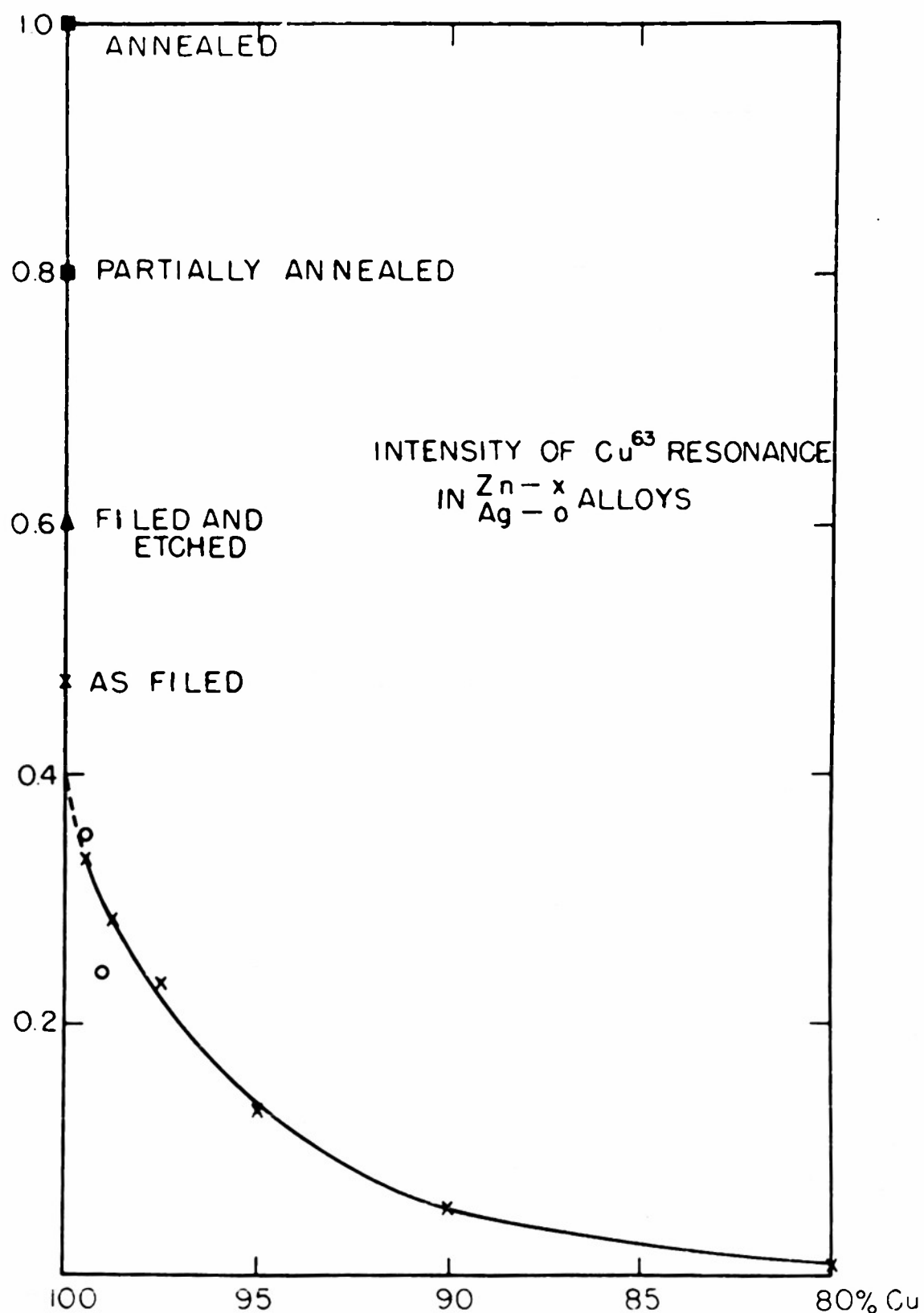


Figure 2 The intensity of the Cu^{63} magnetic resonance in annealed and cold worked copper and in alloys with zinc and silver. By cold work the contribution of the transitions $m_I = \frac{3}{2} \rightarrow \frac{1}{2}$ $m_I = -\frac{1}{2} \rightarrow -\frac{3}{2}$ is washed out. Annealing restores the total intensity of the nuclear resonance.

interaction in one of these 18 positions should then be at least 2.6×10^6 cps as derived from eq. (13). This corresponds to an asymmetry in the wave function around the Cu atom equivalent to 4 per cent an atomic $3d^9 4s^2 {}^2D_{3/2}$ -state or 20 per cent of the atomic $3d^{10} 4p {}^2P_{3/2}$ state.²³ In the case of a neighboring silver atom such a distortion is probably not unreasonable. In the case of a neighboring Zn atom the extra electron may be shared by the surrounding copper atoms, each taking part with an unsaturated covalent bond.²⁴ An excess of a 20 per cent 4p bond in the direction of the Zn atom may not be unreasonable. Townes and Dailey²⁵ have shown that covalent bonding can satisfactorily describe quadrupole coupling in molecules. We leave the question open of what description of distorted orbits will be most appropriate for the metals. Orbital distortion, however, seems to be the dominant origin for quadrupole effects even in alkali halide crystals, strained by the presence of dislocations. Watkins has shown that a calculation based on a distribution of point charges deviating from cubic symmetry does not give the correct answer. A phenomenological multiplication factor β , larger than unity, has to be introduced to obtain results in agreement with the experimental quadrupole coupling.

It can be expected that the shells of the alkali ions will be much less susceptible to deformation than the shells of the transition elements or heavier elements on the right-hand side of the periodic system. In general, the quadrupole interaction provides a serious handicap in the investigation of alloy systems with nuclear spin $I > \frac{1}{2}$. The line-broadening may, however, not be prohibitive for isotopes with small values of the quadrupole interaction like Li^6 and Li^7 . In Li-systems the quadrupole effect could perhaps be studied in detail as the resonance lines may not disappear. The intensity of the nuclear resonance in alloys, if $I > \frac{1}{2}$, gives information about the amount of order in the immediate neighborhood around nuclei with spin $I > \frac{1}{2}$. Tendencies of solute atoms to stay away from each other, the first stages of precipitation and deviations from perfect solid solution or perfect order could be studied in this fashion.

In ordered structures with cubic symmetry the quadrupole broadening should be absent. Attempts to detect the resonance in β -brass near the 50% - 50% composition have failed, presumably because the ordering is not complete.

Also liquid structures should be accessible to investigation as in this case the quadrupole interaction has to be averaged over the rapidly changing configurations and effectively cancels, although there will remain a contribution to the relaxation process. A small quadrupole contribution to the relaxation process is possibly responsible for the fact that the relaxation times for the pairs of isotopes $\text{Ga}^{69} - \text{Ga}^{71}$ and $\text{Rb}^{85} - \text{Rb}^{87}$ have a somewhat smaller ratio than the inverse ratio of the squares of the gyromagnetic ratios for these isotopes.¹¹ It so happens that the isotope with the smaller magnetic moment has the larger quadrupole moment in both cases. For gallium we have

$$\frac{T_1^{69}}{T_1^{71}} = 1.25, \left(\frac{\mu_{71}}{\mu_{69}} \right)^2 = 1.61, \left(\frac{Q_{71}}{Q_{69}} \right)^2 = 0.4.$$

The experimental result is explained if the quadrupole interaction contributes 9 per cent to the relaxation mechanism for Ga^{71} and consequently 35 per cent for Ga^{69} . Since the two rubidium isotopes have different total spin, the comparison is not as straight-forward, and detailed investigation of transitions between the various m-levels would have to be made, not warranted by the experimental uncertainties.

The use of isotopes with spin $I = \frac{1}{2}$, however, avoids all complications of the quadrupole effect. The fact that the intensity of the resonance is not drastically reduced, as in the case of thallium alloys as discussed in a later paragraph, provides perhaps the most convincing proof of the assumption of quadrupole interaction in brass.

3. Nuclear Resonance in Tin, Thallium and Lead

During the first attempts no resonance was found in metallic thallium. If the line width were determined by nuclear dipolar interaction the second moment of the line eq. (7) would be 4.6 kc/s, and the resonance easily observable. The hypothesis was made that the spin-lattice relaxation time would be extremely short and the line correspondingly broader, on account of the very large hyperfine splitting in this element. A broad resonance of 33 kc/s between points of maximum slope (equivalent to 14 gauss) was then found at liquid air temperature. Subsequent investigations showed that the line width was indepen-

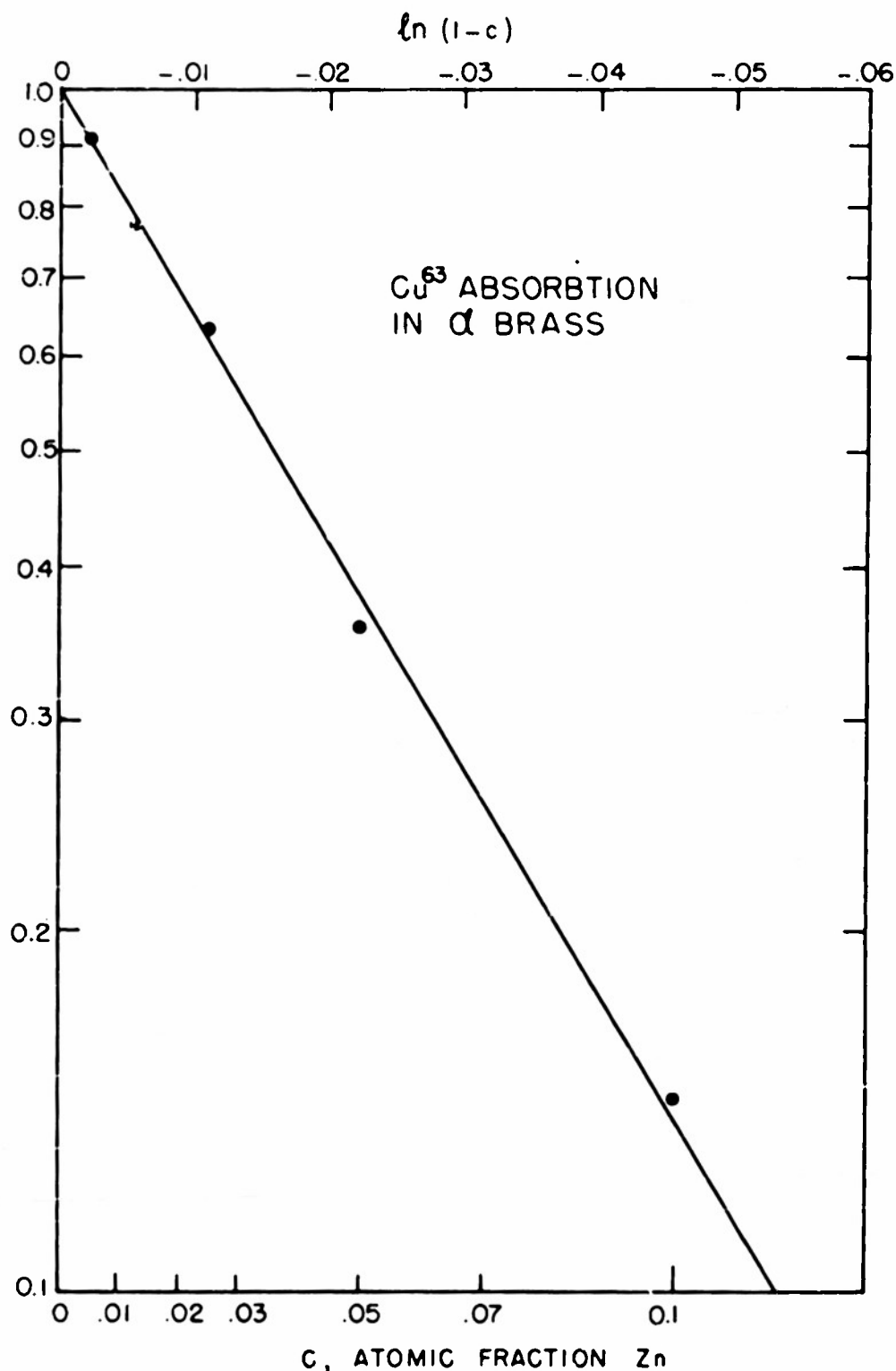


Figure 3. A doubly logarithmic plot of the intensity of the central transition line $m_1 = \frac{1}{2} \rightarrow -\frac{1}{2}$ of Cu^{63} versus zinc concentration C in α -brass. The intensity is normalized to unity for no zinc content. The drawn line $(1 - C)^n$ has a slope corresponding to $n = 18$ with surprisingly good precision. This can be considered as a proof that Zn atom shares an unsaturated covalent bond with the twelve nearest and six next nearest copper atoms only.

dent of temperature in the range from 77°K - 400°K. This seems to rule out the relaxation mechanism as the line-broadening agent. If the conduction electrons are responsible for the relaxation, the line width should be proportional to the absolute temperature. For a Raman scattering process of vibrational lattice phonons a T^2 -dependence would be expected.

It has been suggested by Gutowski¹² that an anisotropy of the Knight shift could be responsible for the width in metals. It will be shown in the next paragraph that the anisotropy, which would have to be about 20 per cent in this case, produces an asymmetrical line with a width proportional to the resonance frequency. Experiments in external fields ranging from 2000 to 6200 gauss revealed no change in the width. Furthermore, the line should become narrow in the cubic phase of thallium, which is stable above 232°C. No resonance was observable above 150°C. If the line had the dipolar width of 4.6 kc/s, it would have been observed. Even more striking is the failure to detect the resonance in the liquid phase, the melting point being at 302°C.

Although the width makes the determination of the line position somewhat inaccurate, the relative Knight shift is so large that it can be measured with fair precision. Figure 4 shows a record of line derivatives of the Tl^{203} and Tl^{205} resonance in fields of about 3000 gauss and 5600 gauss respectively. These resonances were compared with the narrow lines in a saturated aqueous solution of thallium acetate. To what extent these lines can really serve as standards is open to criticism in view of the concentration dependent chemical shift occurring in solutions of thallium salts.²⁶ For Tl^{205} a Knight shift $\Delta\nu/\nu_0 = 1.54\% \pm .05\%$ has been found, the largest so far reported for an element. The behavior of the Tl^{203} resonance is baffling. In going from 2000 to 6000 oersted, the Knight shift changes from 1 per cent to 1.5 per cent, the width changes from 17 kc/s to 33 kc/s and the intensity decreases by a factor three. No such anomalies are observed for the Tl^{205} resonance.

The two isotopes have magnetic moments differing only by 1 per cent and it is not clear how they could behave so differently, if our interpretation of the recordings is at all correct. The preliminary experimental data are mentioned here only for the sake of completeness. Some numerical values are compiled in Table I.

For Pb^{207} in metallic lead a Knight shift of $1.24\% \pm 0.04\%$ has been found. A preliminary value was previously reported by Knight.

The Knight shifts for the resonances of Sn^{117} and Sn^{119} in white tin are 0.74 per cent and 0.72 per cent, which can be considered equal within the experimental error. No values for tin and thallium had been reported previously, a fact undoubtedly due to the unexpected broadness of the lines.

The resonances of Sn^{117} and Sn^{119} in grey tin reveal no Knight shift. It has been shown that the diamond structure of grey tin is semiconducting. The conduction electrons contribute little or nothing to the magnetic susceptibility in this α -phase, $\chi_{\alpha\text{-Sn}} = -0.025 \times 10^{-6}$ and $\chi_{\beta\text{-Sn}} = +0.025 \times 10^{-6}$ cgs units/gram. The contribution to the Knight shift is correspondingly negligible in α -Sn. The number of electrons and holes with unbalanced spin is very small, and furthermore the wave function has predominantly p-character near the top of the valence band and the bottom of the conduction band in the diamond structure. The intensity of the lines for the two isotopes in both modifications is about equal, in agreement with their abundance ratio of 1.08. The lines in α -Sn have a normal shape, but the width is about six times as large as the dipolar broadening. This can clearly not be blamed on the conduction electrons in this semiconducting material.

In the β -modification, however, both resonances have a marked asymmetry. This may be understood as the anisotropy of the Knight shift in the markedly tetragonal white tin structure. A striking confirmation for the correctness of this hypothesis would be to check the proportionality of this asymmetric broadening with the external field. The integrated line, assuming that the recording gives the derivative, is sketched in Figure 6. This line will be interpreted in the next paragraph. The result is that the figures quoted for the Knight shift above are valid, if the field is perpendicular to the tetragonal axis. For fields parallel to the axis the Knight shifts are 0.79 per cent and 0.77 per cent or 7 per cent higher.

4. Anisotropy of the Knight Shift

The first term in the Hamiltonian eq. (6) does not depend on the direction of the external field. The second term produces a shift of the nuclear resonance which depends on the orientation of the external field H_0 with respect

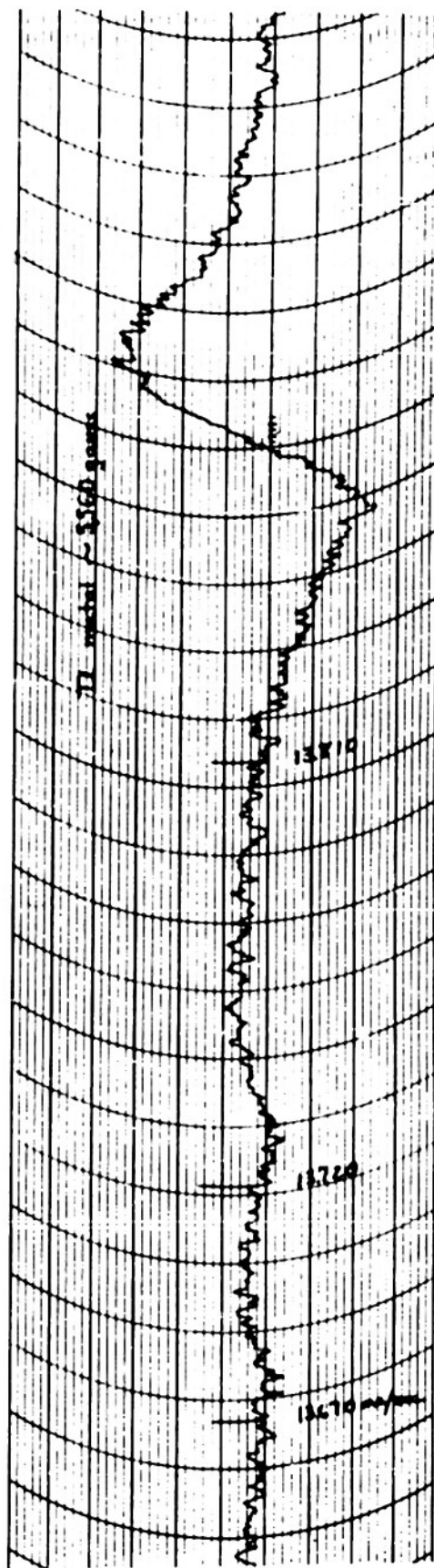
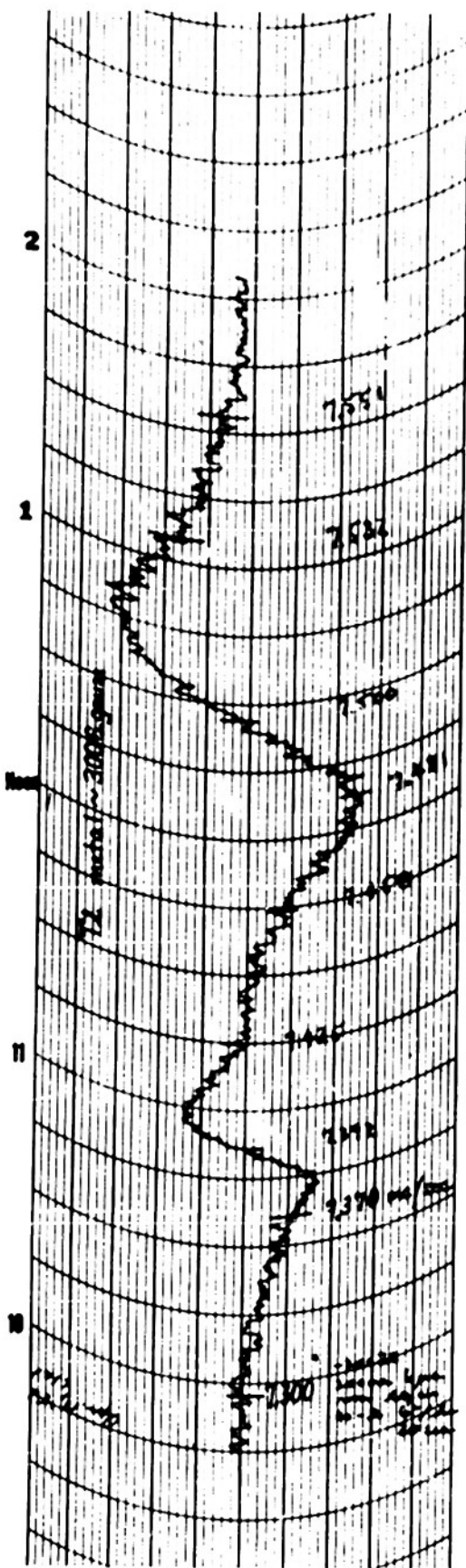


Figure 4 The derivatives of the magnetic absorption in metallic thallium lower curve at 5560 gauss; upper curve at 3006 gauss. The peak at the high-frequency side belongs to the Tl^{205} isotope (relative abundance 70%). The anomalous behavior of the Tl^{203} isotope (relative abundance 30%), which has a magnetic moment only 1.0% smaller than Tl^{205} remains unexplained.

Table I

Sample	Isotope	External Field Strength (Gauss)	Resonance Freq. Mc/s	% Knight Shift		Line Width (Kc/s)	
						obs. *	calc. **
β -Sn	Sn ¹¹⁹	6102	9.761	0.79	11		
	Sn ¹¹⁷	6102	9.323	0.77	11		
	Sn ¹¹⁹	6102	9.756	0.74	<u>1</u>	3-5	.71
	Sn ¹¹⁷	6102	9.319	0.72	<u>1</u>	3-5	
α -Sn	Sn ¹¹⁹	6100.2	9.6786	0.00		5	.75
	Sn ¹¹⁷	6100.2	9.245	0.00		5	
Tl	Tl ²⁰⁵	1993	4.968	1.43 ⁺	.10	30 ⁺ 3	4.6
		3007	7.500	1.50		34 ⁺ 2	
		3665	9.140	1.54		33	
		4890	12.200	1.61		33	
		5563	13.876	1.55		33	
		6108	15.238	1.53		33	
		6495	16.231	1.70		33	
	Tl ²⁰³	1993	4.899	.99		17	3.9
		3050	7.500	1.04		22	
		3720	9.140	1.0 ⁺	.1	28	
		4960	12.200	1.07		35 ⁺ 5	
		5563	13.686	1.11		31	
		6490	16.007	1.33		33	
Pb	Pb ²⁰⁷	5553.4	5.0026	1.24		< 2	.28

|| H₀ parallel to tetragonal axis⊥ H₀ perpendicular to tetragonal axis

* between points of maximum slope

** second moment

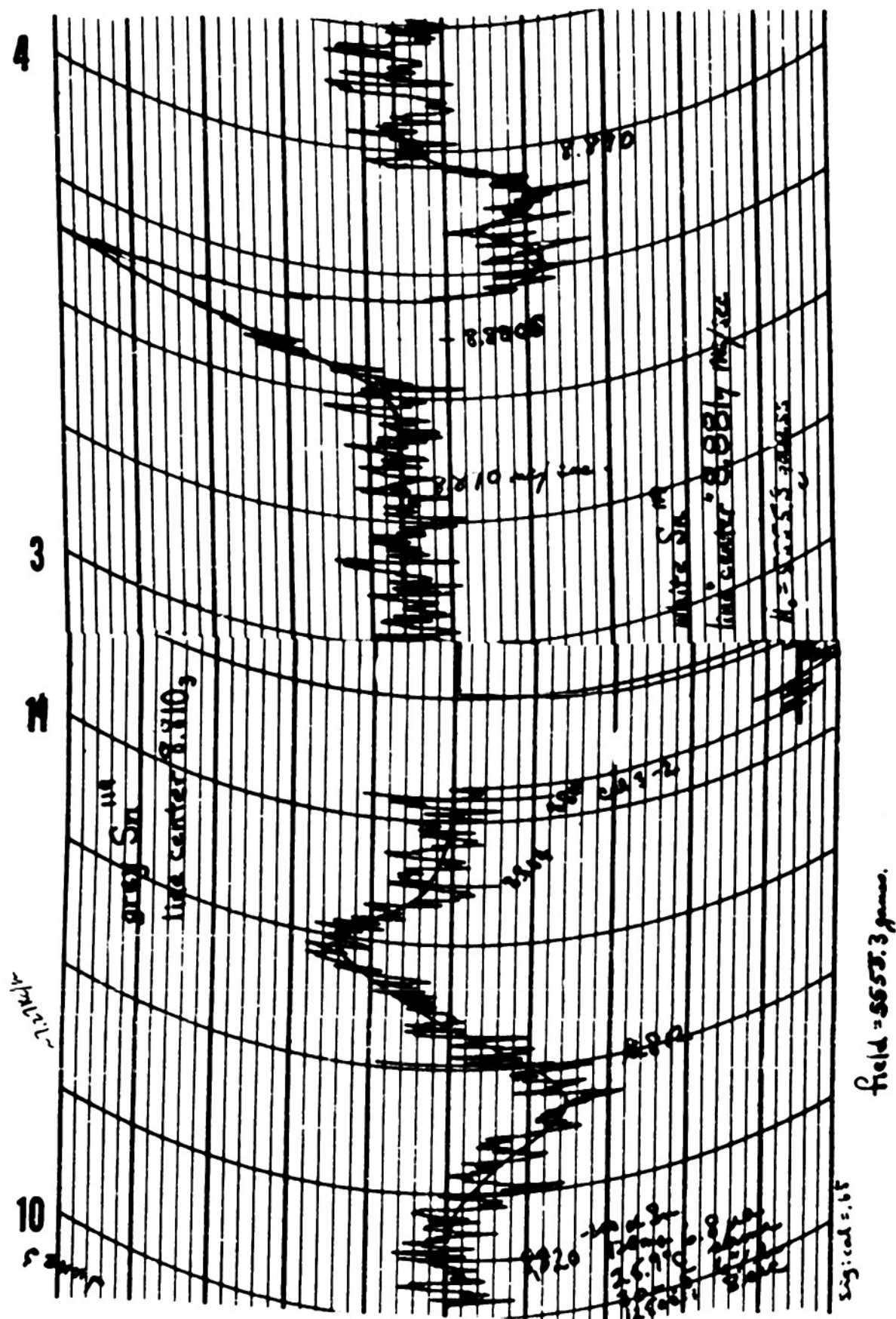


Figure 5 The derivative of the absorption of Sn^{119} in grey tin (diamond cubic) and white tin (tetragonal). The latter curve shows a pronounced asymmetry.

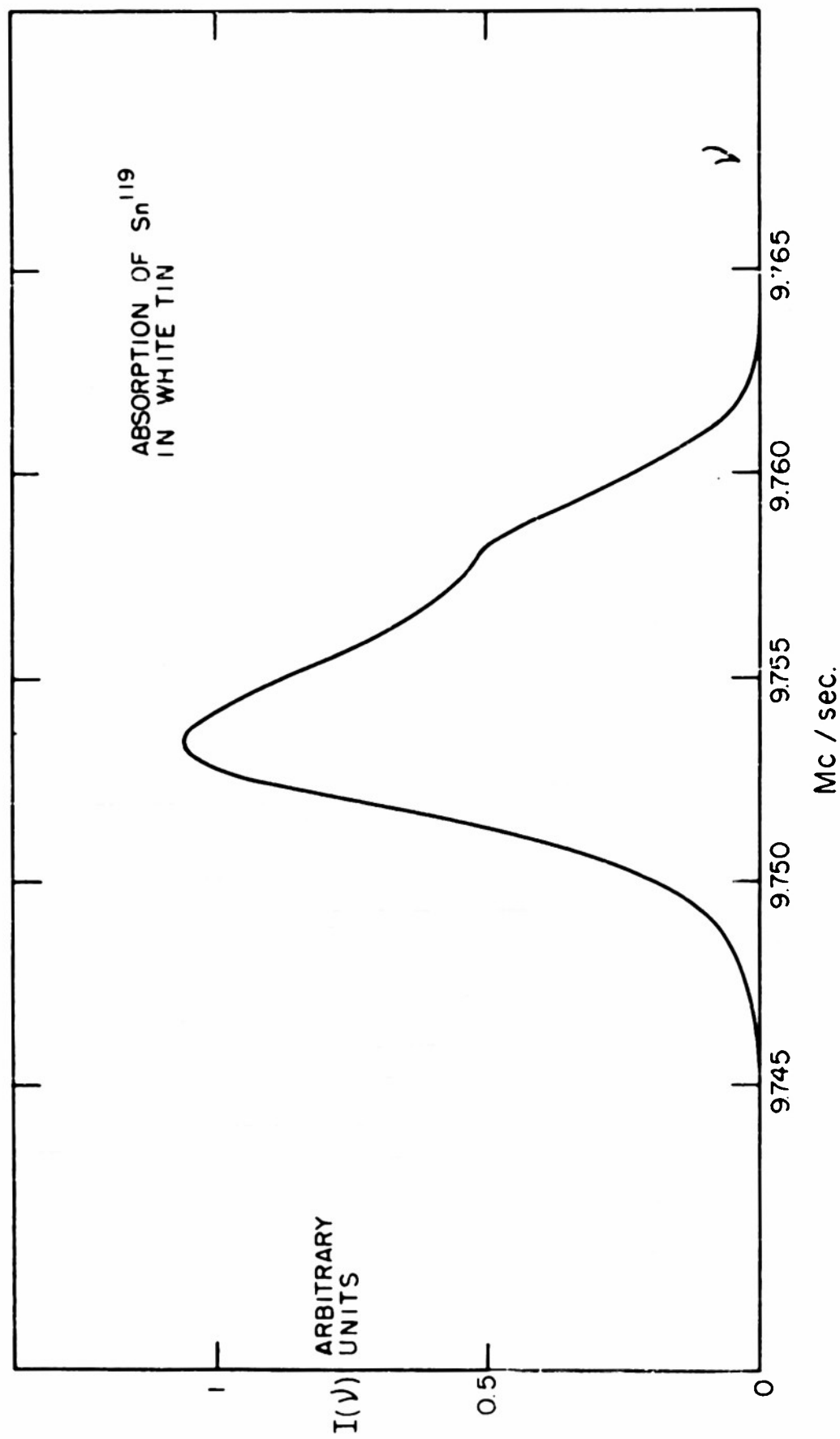


Figure 6 The integrated line shape in tetragonal tin, derived from the recording in Figure 5.

to the crystallographic axes. It vanishes only for cubic symmetry. The third term in eq. (6) can be neglected as the orbital momentum is frozen in. In the first-order perturbation calculation we are only interested in elements diagonal in the nuclear and electron spin. If we denote the angle between H_0 and the radius vector between electron and nucleus by α we retain only the following part of the Hamiltonian

$$\mathcal{H}_{\text{anis}} = \mp \gamma_N \hbar \beta m_I (1 - 3 \cos^2 \alpha) r^{-3} \quad (16)$$

The - or + sign depends on whether the electron moment is parallel or anti-parallel to H_0 respectively. To calculate the shift we determine the energy difference due to eq. (16) between two nuclear spin orientations for which $\Delta m_I = 1$. We have to integrate eq. (16) over the electron wave function ψ_k and then sum over all states k , taking the contributions of electrons of opposite spin with opposite sign. Per unit volume, only $2\beta H_0 N(E_F)$ electrons near the Fermi level with unbalanced spin will therefore contribute. If V_0 is the atomic volume we find for the energy difference

$$\Delta W = \gamma_N \hbar \beta 2 \beta H_0 V_0 N(E_F) \left\langle \int \psi_k^* (3 \cos^2 \alpha_k - 1) r_k^{-3} \psi_k \right\rangle \quad \begin{array}{l} \text{Average} \\ \text{over Fermi} \\ \text{surface} \end{array} \quad (17)$$

If we introduce an average wave function ψ , so that $\psi^* \psi$ represents the average electron density in space of the conduction electrons near the Fermi level, we find from eq. (17) for the relative Knight shift

$$\frac{\Delta H_{\text{anis}}}{H_0} = 2 \beta^2 V_0 N(E_F) \int \psi^* (3 \cos^2 \alpha - 1) r^{-3} \psi dx dy dz \quad (18)$$

The field H_0 makes the polar angles θ and ϕ with respect to the x, y, z coordinate system. The radius vector \underline{r} has polar angles Θ and Φ . We can now express $(1 - 3 \cos^2 \alpha)$ by means of a well-known addition theorem in terms of tesseral harmonics in the angles θ and ϕ and Θ and Φ respectively.

$$\frac{1}{2} (3 \cos^2 \alpha - 1) = \sum_{m=-2}^2 (-1)^m P_2^m(\cos \Theta) P_2^{-m}(\cos \theta) e^{im(\Phi - \phi)} \quad (19)$$

We shall first discuss the case of axial symmetry. It is probably a good approximation to assume that ψ consists of a mixture of p-type wave functions of the form ψ_0 , $\frac{1}{\sqrt{2}} (\psi_{+1} + \psi_{-1})$ and $\frac{1}{\sqrt{2}} (\psi_{+1} - \psi_{-1})$. These wave functions are real and represent the quenching of the p-orbits by the crystalline field. In the case of axial symmetry the electron density can then be written as

$$\psi\psi^* = g(r) \left\{ A(x^2 + y^2) + C z^2 \right\} = r^2 g(r) [A + (C - A) \cos^2 \Theta] \quad (20)$$

Here $g(r)$ is a radial function, whose form is unimportant for our purposes. Clearly eq. (20) could be extended to higher-order terms with axial symmetry, and the following integrations could easily be carried through, if d - or higher orbital states were included. Substituting eqs. (19) and (20) into (18) we find after carrying out the integration over Ω , that only the term with $m = 0$ in eq. (19) contributes, and obtain

$$\frac{\Delta\nu_{\text{anis}}}{\nu_0} = \frac{\Delta H_{\text{anis}}}{H} = \beta^2 V_0 N(E_F) q (3 \cos^2 \Theta - 1) \quad (21)$$

where

$$q = \int \psi (3 \cos^2 \Theta - 1) r^{-3} \psi dV = \frac{16\pi}{15} (C - A) \int_0^\infty r g(r) dr \quad (22)$$

is the quadrupole moment of the electrons near the Fermi level. The interaction with a nuclear quadrupole moment would involve a different quantity q^1 , in which the charges of all electrons and nuclei are involved and not just the charges of the conduction electrons near the Fermi level.

The shift eq. (21), which averages to zero for a polycrystalline material, is, of course, superimposed on the isotropic shift $\Delta\nu_{\text{is}}$ given by eq. (3).

It is to be noted that the angular dependence of eq. (21) is the same, as could be inferred in a purely phenomenological way, if one assumes that a linear tensor relation exists between the internal field ΔH and the external field H_0 . Since in first-order approximation only the component of ΔH parallel to H_0 will alter the resonance frequency we can write down immediately

$$\Delta\nu = \Delta\nu_{11} \cos^2 \Theta + \Delta\nu_{\perp} \sin^2 \Theta \quad (23)$$

The phenomenological quantities $\Delta\nu_{11}$ and $\Delta\nu_{\perp}$ can be identified as

$$\Delta\nu_{11} = \Delta\nu_{is} + 2\beta^2 v_o N(E_F) q v_o$$

$$\Delta\nu_{\perp} = \Delta\nu_{is} - \beta^2 v_o N(E_F) q v_o$$

The number of nuclei in the powdered specimen, for which the magnetic field makes an angle θ with the crystallographic z -axis is, of course, proportional to $\sin \theta$. This distribution over angles must be transformed into a distribution function over resonance frequencies. The straight-forward procedure is the same as used, e.g., by Pake²⁷ for the shape of the resonance of the two-proton systems in powders. Using eq. (23) we find for the line intensity

$$\mathcal{I}(\nu) \propto \sin \theta \left(\frac{d\nu}{d\theta} \right)^{-1} \propto \left| \nu - \nu_o - \Delta\nu_{\perp} \right|^{-1/2} \quad \text{if } \Delta\nu_{11} > \nu - \nu_o > \Delta\nu_{\perp}$$

or

$$\mathcal{I}(\nu) \propto (\Delta\nu_{\perp} + \nu_o - \nu)^{-1/2} \quad \text{if } \Delta\nu_{\perp} > \nu - \nu_o > \Delta\nu_{11}$$

$$\mathcal{I}(\nu) = 0 \quad \text{outside this interval.} \quad (24)$$

The line shape $\mathcal{I}(\nu)$ is given by the dotted line in Figure 7 for the case $\Delta\nu_{11} > \Delta\nu_{\perp}$, corresponding to a positive value of q . Dipolar broadening and finite life-time will change the distribution to one indicated by the solid line. This is in excellent agreement with the line shape observed in tetragonal tin. We conclude therefore that q is positive. The dominant contribution to the gradient of the electric field at the nucleus comes from electrons along the tetragonal axis. This agrees with the crystal structure²⁸ where the four nearest neighbors form a tetrahedron, squashed in the direction of the tetragonal axis, while the two next nearest neighbors are in the direction of the tetragonal axis. If one assumes a uniform charge distribution around each nucleus, it is elongated along the tetragonal axis. The experiment gives for the anisotropy

$$\frac{\Delta\nu_{11} - \Delta\nu_{\perp}}{\nu_o} = 0.05\%$$

We calculate $N(E_F)$ from the electronic specific heat data^{21,29} with the result that $V_0 N(E_F) = 0.19 \times 10^{12} \text{ erg}^{-1}$. Substituting these values into eq. (23), we obtain $q = + 8.8 \times 10^{24} \text{ cm}^{-3}$. The relative anisotropy of the shift $(\Delta_{11} - \Delta_{11})/\Delta_{11}$ amounts to 7 per cent. This should be considered as large. The \bar{p} -character of the wave function must be appreciable. The hyperfine interaction in the p-state is smaller than in the s-state, and furthermore we detect only the anisotropy in the p-wave functions. The total amount of p-character should well exceed 50 per cent near the Fermi level in white tin.

In hexagonal structures where the nearest neighbors have a nearly cubic arrangement, much smaller anisotropies should be expected, and in fact no other asymmetric lines have been reported. The asymmetry should become more pronounced in higher fields. The problem treated here is somewhat similar to the dipolar interaction in solid hydrogen treated by Reif.³⁰ For the proton-spin pair a symmetric line always results because the spin of the proton has equal probability for parallel or antiparallel orientation. In our problem of the nuclear spin-electron spin-pair interaction, we have to take the average value of the electron spin moment, as the motion of the electrons is much more rapid than the nuclear precession frequency. The net moment is always oriented parallel to H_0 . This leads to an asymmetric broadening, proportional to the value of H_0 . These two features enable us to distinguish the anisotropic Knight shift from quadrupole interactions, in case the nuclear spin $I > \frac{1}{2}$. It is interesting that a value q for the upper conduction electrons can be derived from this effect, but this is of no direct avail in the absolute determination of nuclear quadrupole moments. As pointed out before, another q involving the total charge distribution is effective in that case.

The derivation for the anisotropy of the Knight shift showed no relation with the anisotropy in the observed magnetic susceptibility. The latter is mostly due to diamagnetic effects of the orbital motion. It is possible that some anisotropy in the Pauli spin paramagnetism occurs because of an anisotropic g-factor. If the spin-orbit coupling due to the partial "non-s character" in the wave function is appreciable compared to crystalline field splittings in the conduction band, one will have a g-factor

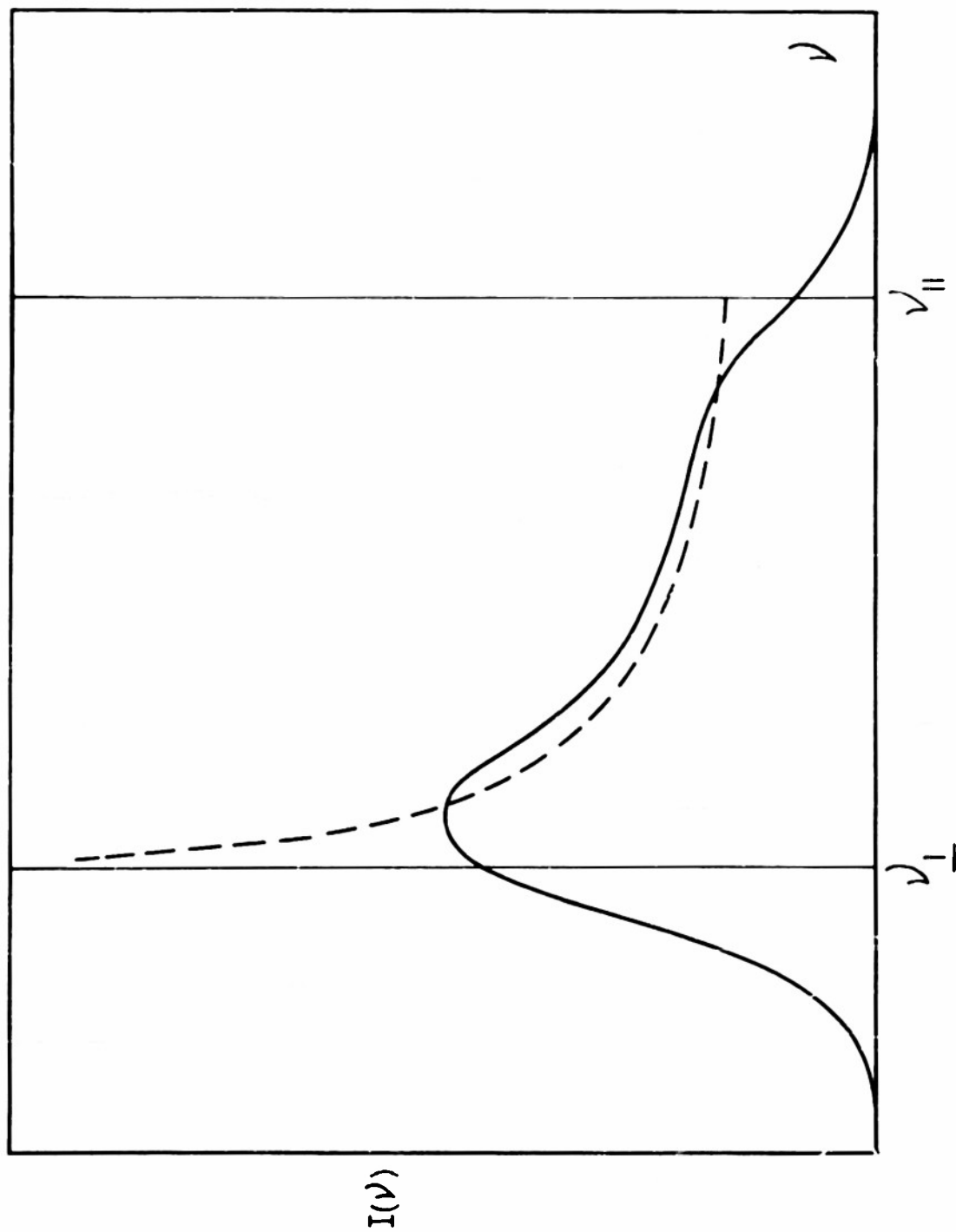


Figure 7. The theoretical line shape in a polycrystalline powder due to the anisotropy of the Knight shift in an axially symmetric conductor (dotted curve). The drawn curve gives the experimental line shape, if dipolar interaction and other causes of symmetric line broadening are superimposed.

different from 2, and in a tetragonal crystal one has to distinguish between g_{11} and g_1 . The partial s character of the wave function then leads, according to eq. (3), to an anisotropy in the Knight shift

$$\frac{\Delta\nu_{11} - \Delta\nu_1}{\nu_0} = \frac{(g_{11} - g_1) \beta I}{2\mu_N} C A V_c N(E) \quad (24a)$$

This anisotropy effect should be added algebraically to that given by eq. (21). Phenomenologically the two effects are indistinguishable. It will be very difficult to obtain experimental information about g_{11} and g_1 . In the absence of a theoretical evaluation we have used eq. (21) only to obtain a value for q . This will be incorrect, if the anisotropy is several per cent. This would still require a sizeable amount of "non-s character" of the wave function, but perhaps less than the use of eq. (21) would indicate. The anisotropic diamagnetic susceptibility will of course give rise to an anisotropic magnetic shielding of the nuclei. But the order of magnitude of this effect is much smaller, perhaps a few parts in a million.³¹

We finally extend the preceding considerations to the general case when there is no axis of symmetry. Instead of eq. (20) we now have for the average density of the conduction electrons near the Fermi level

$$\psi\psi^* = g(r)(Ax^2 + By^2 + Cz^2) \quad (25)$$

Substituting eqs. (19) and (25) into eq. (18) one finds that $\Delta\nu_{\text{anis}}$ is now not only a function of θ , but also of ϕ .

$$\frac{\Delta\nu_{\text{anis}}}{\nu_0} = 2\beta^2 V_0 N(E_F) \left\{ \left(C - \frac{1}{2}A - \frac{1}{2}B \right) \frac{8}{15}\pi (3\cos^2\theta - 1) + \frac{4}{5}\pi(A-B)\sin^2\theta \cos 2\phi \right\} \int_0^\infty r g(r) dr \quad (26)$$

This expression reduces properly to eq. (21) for $A = B$.

In order to calculate the line shape we introduce three frequencies

ν_1 , ν_2 and ν_3 , at which the resonance occurs, if H_0 points along one of the axes. We assume without loss of generality that $\nu_3 > \nu_2 > \nu_1$. The resonance frequency for the direction θ , ϕ is then given by

$$\nu = \nu_1 \sin^2 \theta \sin^2 \phi + \nu_2 \sin^2 \theta \cos^2 \phi + \nu_3 \cos^2 \theta \quad (27)$$

A comparison with eq. (26) readily relates these phenomenological quantities with the A, B and C and with the isotropic shift $\Delta\nu_{is}$. We first calculate from eq. (27) what the line shape would be if θ were held fixed

$$\mathcal{J}'(\nu, \theta) \propto \left(\frac{\partial \nu}{\partial \phi} \right)^{-1} \propto (\nu - \nu_3 \cos^2 \theta - \nu_1 \sin^2 \theta)^{-1/2} (-\nu + \nu_3 \cos^2 \theta + \nu_2 \sin^2 \theta)^{-1/2}$$

for

$$\frac{\nu - \nu_1}{\nu_3 - \nu_1} > \cos^2 \theta > \frac{\nu - \nu_2}{\nu_3 - \nu_2} \quad \text{if } \nu_2 < \nu < \nu_3$$

and

$$\frac{\nu - \nu_1}{\nu_3 - \nu_1} > \cos^2 \theta > 0 \quad \text{if } \nu_1 < \nu < \nu_2$$

and zero outside these intervals for θ . To find the actual shape we have to integrate over the permissible range of θ values

$$\mathcal{J}(\nu) = \int \mathcal{J}'(\nu, \theta) \sin \theta \, d\theta$$

and find after some manipulation that $\mathcal{J}(\nu)$ can be brought into the form of the complete elliptic integrals.

$$\mathcal{J}(\nu) \propto \sqrt{\frac{\nu_3 - \nu_1}{\nu - \nu_1}} \int_0^{\pi/2} \left\{ 1 - \frac{(\nu_2 - \nu_1)(\nu_3 - \nu)}{(\nu_3 - \nu_2)(\nu - \nu_1)} \sin^2 \gamma \right\}^{-1/2} d\gamma \quad \text{for } \nu_2 < \nu < \nu_3 \quad (28)$$

$$\mathcal{J}(\nu) \propto \sqrt{\frac{(\nu_3 - \nu_1)(\nu_3 - \nu_2)}{(\nu_3 - \nu)(\nu_2 - \nu_1)}} \int_0^{\pi/2} \left\{ 1 - \frac{(\nu - \nu_1)(\nu_3 - \nu_2)}{(\nu_3 - \nu)(\nu_2 - \nu_1)} \sin^2 \gamma \right\}^{-1/2} d\gamma \quad \text{for } \nu_1 < \nu < \nu_2$$

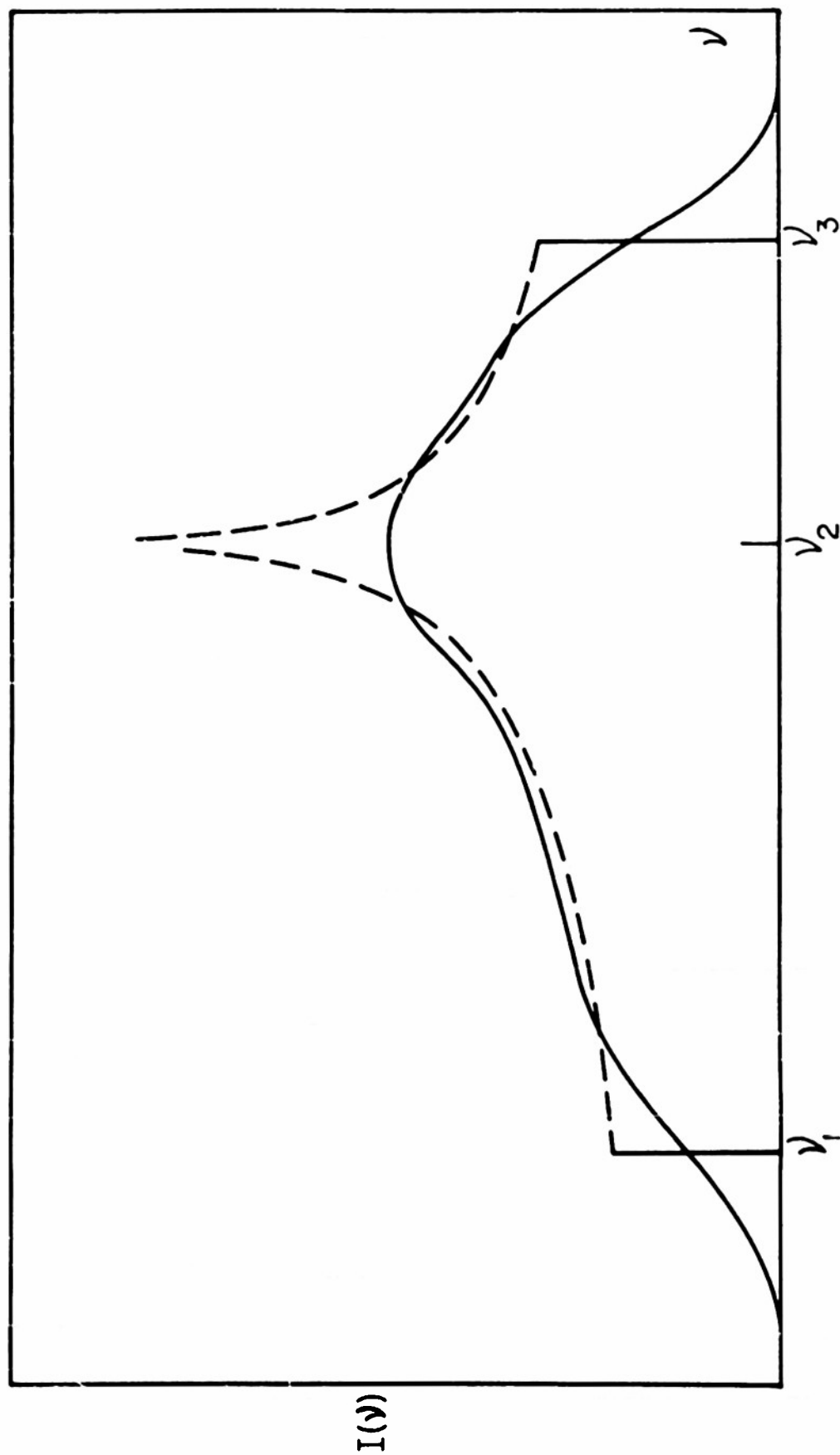


Figure 8 The theoretical line shape in a polycrystalline powder due to anisotropy of the Knight shift in a conductor with less than axial symmetry. The drawn curve includes the symmetric broadening by dipolar interaction and finite relaxation time.

$$\mathcal{J}(\nu) = 0$$

$$\text{for } \nu < \nu_1$$

$$\nu > \nu_3$$

The line shape has been plotted in Figure 8, for the case $\frac{1}{2}(\nu_2 - \nu_1) = \nu_3 - \nu_2$.³² The values of the elliptic integrals can be found in the tables of Jahnke — Emde.³² There is a logarithmic divergence at the frequency ν_2 . Further broadening of the line by dipolar interaction will smooth this out almost completely, and the real line shape is indicated by the drawn line. Note that the line would be symmetrical, if $\nu_3 - \nu_2 = \nu_2 - \nu_1$. No observations on a metal with less than axial symmetry have been made. It would be interesting if such a line shape could be identified.

5. The Nuclear Resonance in Thallium Alloys

After the line in metallic thallium had been found, experiments on thallium alloys were immediately successful. The lines retained their intensity, as quadrupole effects are absent. The width varied somewhat in the different alloys, but not by spectacular amounts. An exception is perhaps formed by the thallium-bismuth alloys where the line width increased by a factor 3 to 110 kc/s. A remarkable result was obtained in a liquid alloy (90% Hg, 10% Tl) at room temperature. The width has the same order of magnitude as in the solid phases and is apparently not narrowed by the rapid motion in the liquid. This is all the more remarkable as a spin lattice relaxation mechanism is again ruled out by the lack of variation with temperature.

Data on the width and Knight shift are assembled in Table II. The Knight shift exhibits appreciable variations on alloying. In one phase it changes continuously with composition. This behavior is illustrated for the thallium-tin system in Figure 9. The solubility of thallium in tin is too small to obtain data at the other end of the phase diagram. The relative shift increases from 1.54 per cent in pure thallium to 1.97 per cent at the phase boundary. The Knight shift of tin in the alloy (20% Sn-80% Tl) on the other hand is smaller (0.67%) than in pure tin (0.75%). According to eq. (3) the variation can be caused by a change in the quantities C , V_0 and $N(E)$. In a first approximation it is probably correct to assume that CV_0 is constant, as the hyperfine interaction normalized per atom is inversely

proportional to the atomic volume V_0 . Then the plot of the Knight shift is also a plot of density of states near the Fermi level $N(E_F)$. For a free electron gas this quantity is proportional to $E_F^{1/2}$. It is plausible that the addition of tin to thallium raises the number of conduction electrons per unit volume and consequently E_F and $N(E_F)$. There are some data on the magnetic susceptibility which also indicate an increase of $N(E)$. The specific susceptibility increases from $\chi_{Tl} = -0.22 \times 10^{-6}$ to $\chi_{80\% Tl + 20\% Sn} = -0.11 \times 10^{-6}$. The density $N(E)$ levels off near the phase boundary; a decrease which might be expected according to Jones' explanation³³ of the Hume-Rothery rules is not observed. Additions of less than 3 per cent tin do not change the Knight shift. The density of states $N(E_F)$ remains constant at first and increases only when more than 3 per cent tin is added. This is in agreement* with Friedel's theory of impurities in metals.³⁴ The tin atoms in small concentration act like impurities, which have either a bound electron or a compressed Fermi gas of conduction electrons around them. In either case the maximum momentum k_M , and therefore $N(E_F)$, are unchanged. For higher concentrations the impurities interact and $N(E_F)$ increases.

The line width increases by a factor two if 10 per cent tin is added. Data are given in Figure 10. The thallium nuclei in the solid solution do not all have the same environment. There will be a certain distribution in the value of $|\psi(0)|^2$, depending on the presence of tin atoms in the immediate neighborhood. This will lead to a distribution of Knight shifts. Although one would expect an asymmetric distribution for small tin concentrations, an asymmetric broadening has not been observed.

Discontinuities in the Knight shift occur when phase transitions take place. In the two-phase regions of the phase diagram the resonance will therefore be double. This is illustrated in Figure 11, where the Knight shift is plotted versus composition of thallium-mercury alloys. The relative change in the Knight shift is more than 70 per cent in going from the β - to the γ -phase. The change is partly caused by volume effects but mostly by electronic structure. Another example of the effect of phase change on the Knight shift is the melting of Tl-Hg alloys. A pure increase in volume would

* Professor Brooks first proposed this explanation.

Table II

System	Phase or Composition	Isotope	Knight Shift	Line Width (Kc/sec)	
				exptl.*	calc.**
Na-Tl	pure Tl	Tl ²⁰⁵	1.54 [†] .05	33	4.6
	NaTl	Tl ²⁰⁵	-1.03	50	
	Na ₂ Tl	Tl ²⁰⁵	.68	38	
Mg-Tl	NaTl	Na ²³	- .016	3.4	2.0
	MgTl	Tl ²⁰⁵	2.12	40	
In-Tl	50 At. % In-Tl	Tl ²⁰⁵	1.68	38	
Sn-Tl	0-25 At. % Sn-Tl	Tl ²⁰⁵	1.54 to 1.97	33-64	
	see detailed shift vs. composition data				
Hg-Tl	25 At. % Sn-Tl	Sn ¹¹⁹	.67	5	
	pure β -Sn	Sn ¹¹⁹	.74	5	0.71
	pure α -Sn	Sn ¹¹⁹	0.0	5	0.76
Pb-Tl	13 At. % Hg-Tl	Tl ²⁰⁵	1.71	34	
	60 At. % Hg-Tl	Tl ²⁰⁵ (liquid)	1.49	20	
	72 At. % Hg-Tl	Tl ²⁰⁵	1.01	33	
	92 At. % Hg-Tl	Tl ²⁰⁵ (liquid)	1.18	(30)	
Bi-Tl	34 At. % Pb-Tl	Tl ²⁰⁵	1.39	34	
	90 At. % Pb-Tl	Tl ²⁰⁵	1.90	33	
	pure Pb	Pb ²⁰⁷	1.24	<2	0.28
Bi-Tl	6 At. % Bi-Tl	Tl ²⁰⁵	1.71	75	
	19 At. % Bi-Tl	Tl ²⁰⁵	1.74	110	
	59 At. % Bi-Tl	Tl ²⁰⁵	1.1	110	

* between points of maximum slope

** second moment

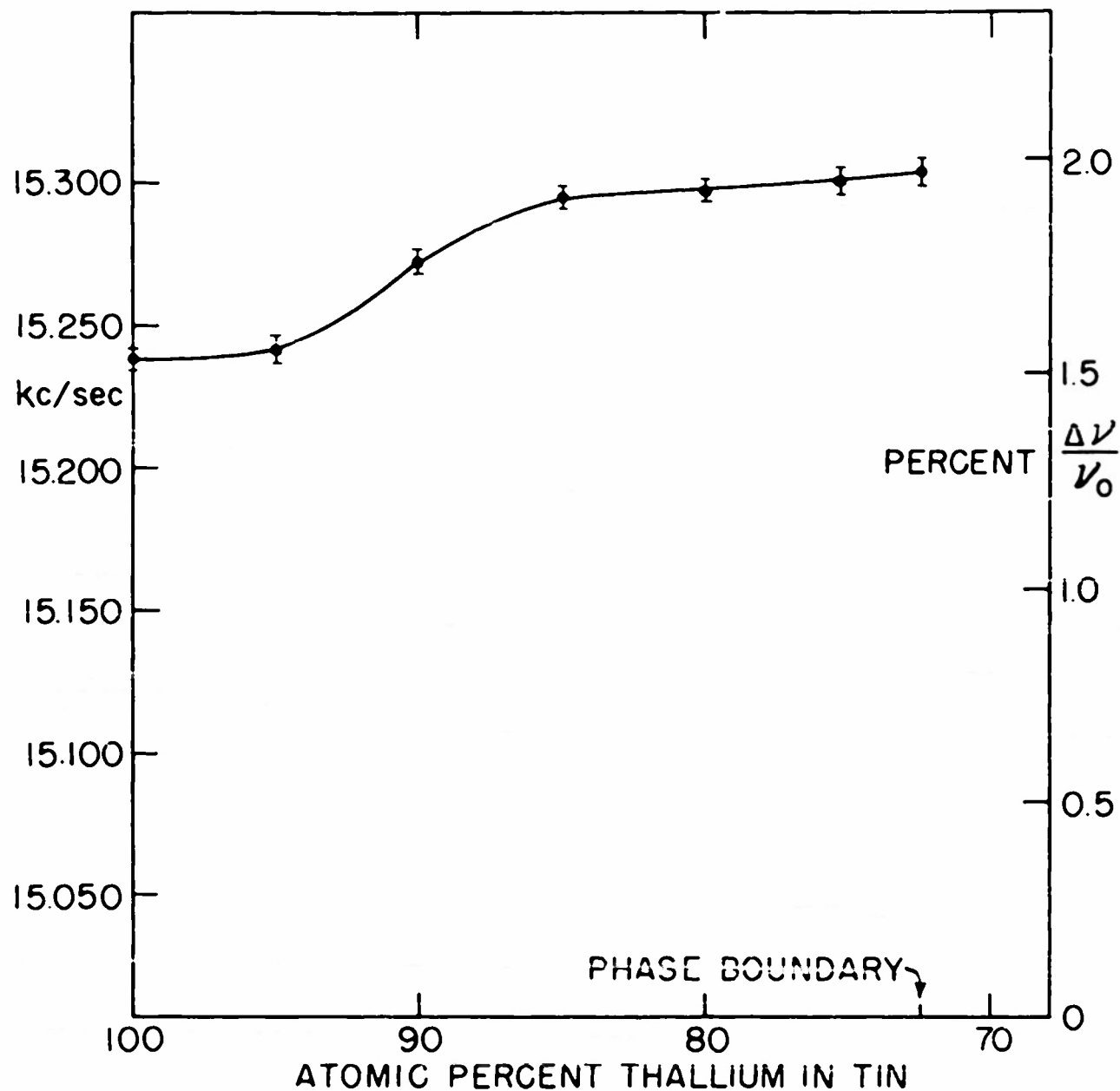


Figure 9 The shift of the Tl^{205} resonance in solid solutions of tin in thallium. The fact that tin concentrations less than 3% have no effect on the Knight shift can be considered as proof of Friedel's theory of impurity levels in metals, which leave the Fermi level unaffected. For higher concentrations the curve represents the filling up of the conduction band and gives the density of electron states $N(E)$.

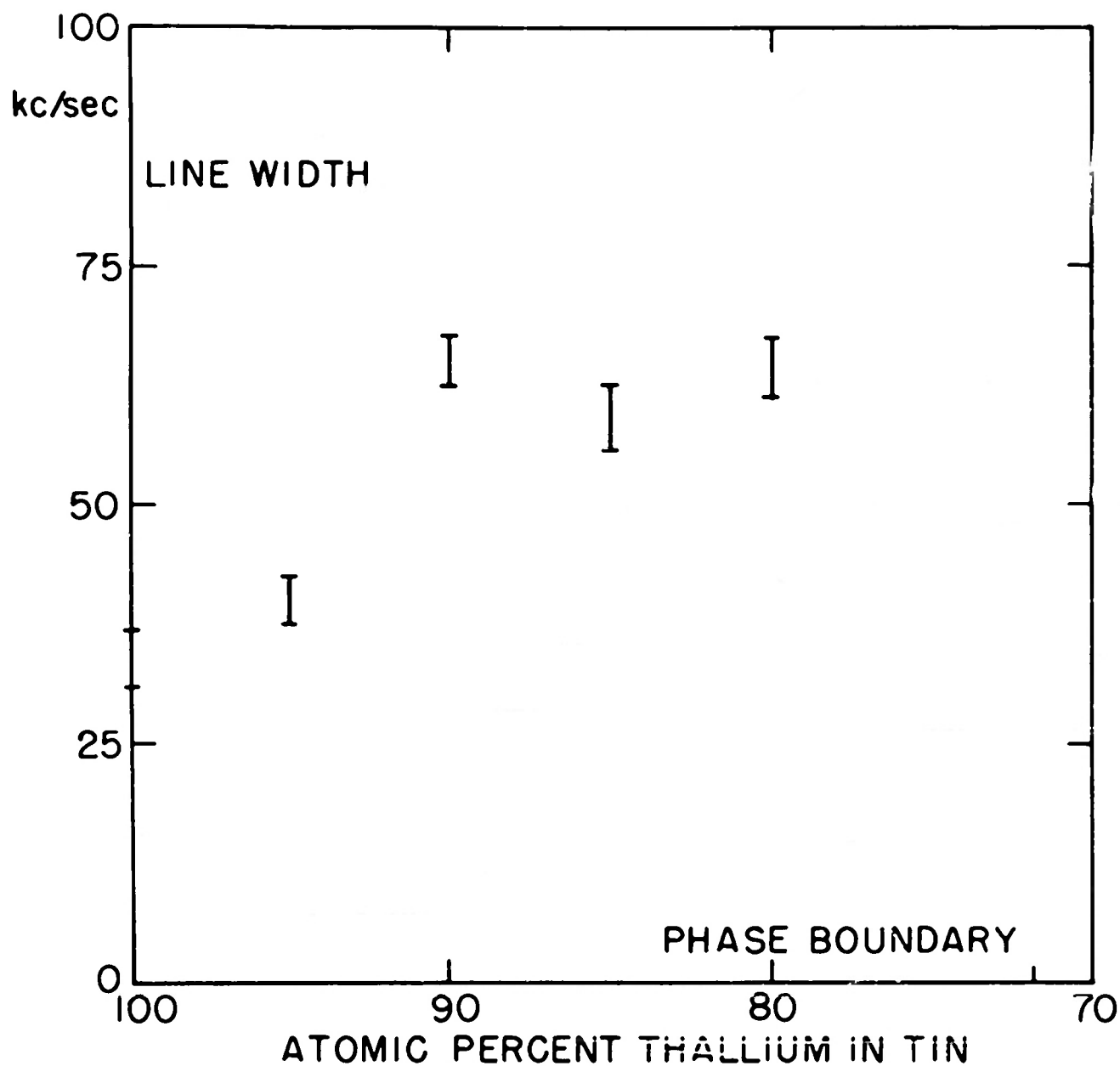


Figure 10 The line width, measured between points of maximum slope, in solid solutions of tin in thallium.

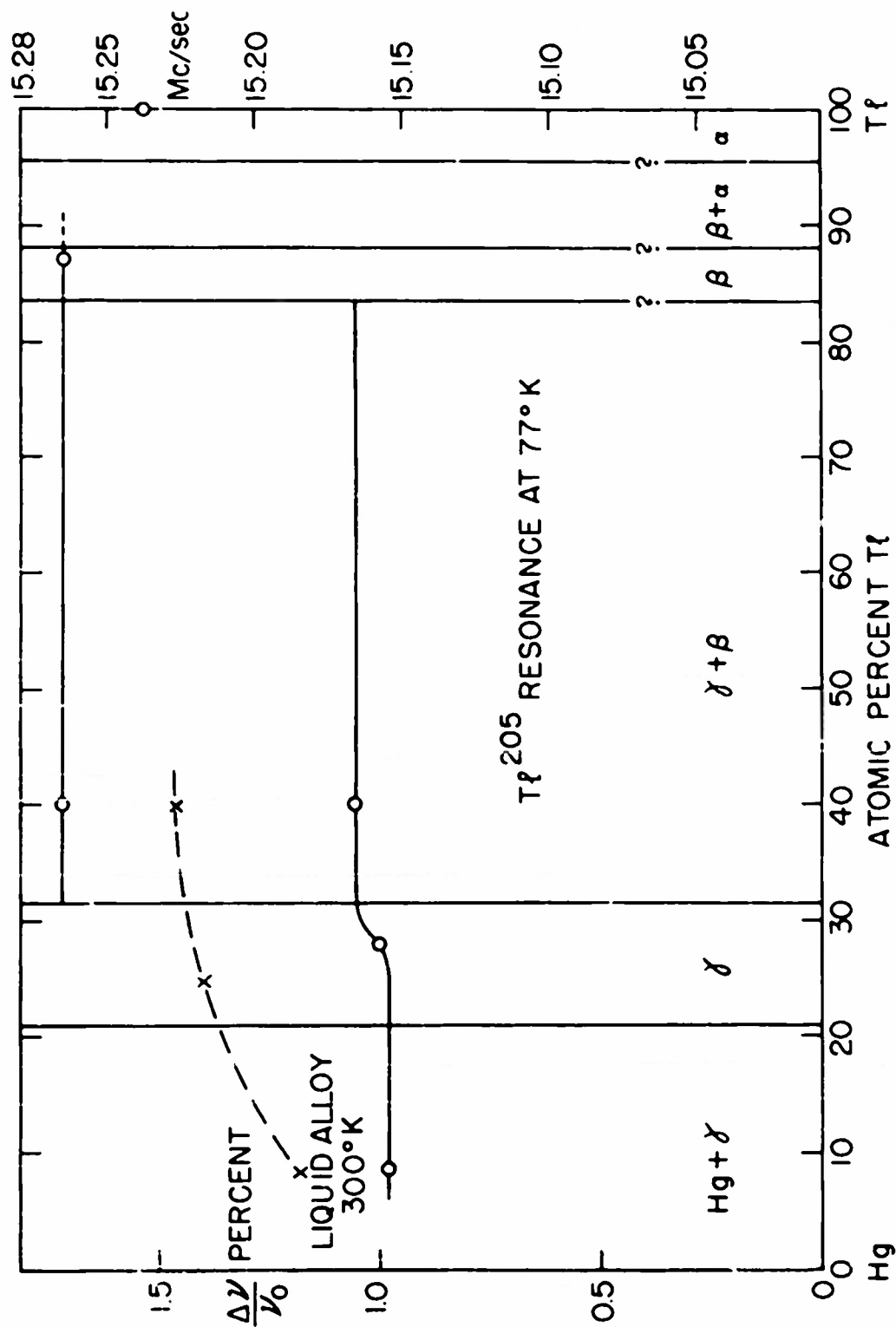


Figure 11 The shift of the Tl^{205} resonance in thallium mercury alloys. In the two-phase regions two resonance lines occur. In the $\beta + \alpha$ region an unresolved line, presumably consisting of two components was observed, but is not indicated in the figure. The dotted line refers to the resonance at $24^\circ C$ in liquid alloys. Discontinuities occur in the transition from one solid phase to another and to the liquid phase. The indicated phase boundaries do not apply to the liquid phase.

presumably lower the Knight shift according to eq. (3). Actually, an increase of 20 per cent is observed on melting, indicating a change in the electronic structure. The behavior of the Knight shift over the phase diagram is roughly what could be expected. The knowledge of the electronic structure of these alloys is, however, insufficient to attempt a quantitative explanation.

A thallium-magnesium alloy exhibits the largest Knight shift of 2.1 per cent.

A most remarkable result was obtained in the ordered Na Tl structure. This intermetallic compound shows a negative Knight shift (-1.03%) for thallium. Since it is an ordered structure with cubic symmetry, the Na²³ resonance could also be observed, and it shows a small shift towards lower frequencies. A shift of -0.016 per cent was found compared to a solution of Na I. In metallic sodium an ordinary positive shift of 0.11 per cent occurs. We have not yet performed experiments at other frequencies and do not know whether the shift is really proportional to ν_0 , although it seems unlikely that a chemical shift would be this large. Experiments on other alloys with the Na Tl structure are also planned.

A possible explanation of the negative shift might perhaps be found along the following lines. Abragam and Pryce³⁵ have shown that Mn⁺⁺ ions, and other ions of the iron group, exhibit configurational interaction, in which a 3s-electron is promoted to the 4-s orbital. The total spin or the magnetic moment of the ion is not changed by this promotion, but the interaction with the nucleus is changed. The electron spin interacts more strongly in the 3 s orbit than in the 4-s orbit. The effective spin density at the nucleus due to the unpaired s-electrons is determined by overlap integrals of radial wave functions. This configurational interaction accounts for the hyperfine structure of the Mn⁺⁺-ion. Abragam and Pryce^{*36} show that it is proportional to the amplitude of the admixed wave function and not to its square. It is an interference effect which actually gives a negative sign for the $\mathbf{A} \cdot \mathbf{I} \cdot \mathbf{S}$ interaction in the Mn⁺⁺ ion. The question is whether configurational interaction in a metal might cause some mixing with a state in which an inner s-electron is promoted to higher orbits in the conduction band with s-wave character, and whether this effect would yield a particularly

* - - - - -

The authors are indebted to Dr. Abragam for calling their attention to this effect and for making the manuscript available before publication.

large negative value for Na Tl. Clearly much theoretical work and more experimental data are needed to confirm this hypothesis. The width of the Na²³ resonance in Na Tl is normal. It should be remembered that the tabulated experimental and theoretical values are not directly comparable. The width of the thallium resonance is, however, of the same order of magnitude as found in all other samples. This is another argument that the anomalously large width is a characteristic of the atomic configuration of the heavy elements, rather than of the electronic structure of the conduction band.

Unfortunately, we have no data on the spin-lattice relaxation time for any of the observed resonances. No check on the validity of the Korringa relation is therefore possible.

The authors wish to express their indebtedness to Professors H. Brooks, J. Friedel, H. Jones and Dr. C. Herring for several valuable discussions. One of the authors (T.J.R.) acknowledges a stipend from the California Research Corporation.

References

1. W. D. Knight, Phys. Rev. 76, 1259 (1949)
2. C. H. Townes, C. Herring and W. D. Knight, Phys. Rev. 77, 852 (1950)
3. E. Fermi, Z S f Phys 60, 320 (1930)
4. W. Kohn and N. Bloembergen, Phys Rev 80 913 (1950), 82, 283 (1951)
5. W. Heitler and E. Teller, Proc Roy Soc A 155, 637 (1936)
6. J. Korringa, Physica 16, 601 (1950)
7. A. W. Overhauser, Phys Rev 89, 1316 (1953)
8. N. Bloembergen, Physica 15, 588 (1949)
9. N. J. Poulis, Physica 16, 373 (1950)
10. J. Hutton and B. V. Rollin, Proc Roy Soc A 199, 222 (1949)
11. H. S. Gutowski and B. R. McGarvey, J Chem Phys 20, 1472 (1952)
12. H. S. Gutowski, Phys Rev 83, 1073 (1951)
13. R. E. Norberg and C. P. Slichter, Phys Rev 83, 1075 (1951)
14. R. V. Pound and W. D. Knight, Rev Sci Ins 21, 219 (1950)
15. C. Watkins, Thesis, Harvard University (1952)
16. N. Bloembergen, J App Phys 23, 1383 (1952)
17. R. V. Pound, Phys Rev 79, 685 (1950)
18. R. V. Pound, J Phys Chem (to be published)
19. B. Bleaney, K. D. Bowers and R. S. Trenam, Proc Phys Soc 66 A, 410 (1953)
20. N. F. Mott and H. Jones, THE THEORY OF THE PROPERTIES OF METALS AND ALLOYS pp 86-88, Oxford University Press, 1936
21. N. F. Mott, Prog in Metal Phys 3, 76 (1952)
22. K. Huang, Proc Phys Soc 60, 161 (1948)
23. P. Brix and H. Kopfermann, Landolt-Bornstein, Zahlenwerte und Funktionen I.5
24. L. Pauling, Proc Roy Soc A 196, 343 (1949)
25. B. P. Dailey and C. H. Townes, J Chem Phys 17, 782 (1949)
26. H. S. Gutowski and B. R. McGarvey, Phys Rev 91, 81 (1953)
27. G. E. Pake, J Chem Phys 16, 327 (1948)
28. Wyckoff, CRYSTAL STRUCTURES, Interscience Publishers, New York
29. W. H. Keesom and P. H. van der Laer, Physica 5, 193 (1938)
30. F. Reif, Thesis, Harvard University (1953)
31. N. F. Ramsey, Phys Rev 86, 243 (1952)

32. E. Jahnke and F. Emde, TABLES OF FUNCTIONS, Dover Publications, New York, 1945
33. N. F. Mott and H. Jones, loc. cit. pp170-173
34. J. Friedel, Phil Mag 43, 153 (1952)
35. A. Abragam and M. H. L. Pryce, Proc Roy Soc A 205, 135 (1951)
36. A. Abragam and M. H. L. Pryce, to be published.

DISTRIBUTION

2	Office of Naval Research (427) Navy Department Washington 25, D. C.
1	Office of Naval Research (460) Navy Department Washington 25, D. C.
1	Chief, Bureau of Ordnance (Re4f) Navy Department Washington 25, D. C.
2	Chief, Bureau of Ships (810) Navy Department Washington 25, D. C.
1	Chief, Bureau of Aeronautics (EL-51) Navy Department Washington 25, D. C.
1	Chief of Naval Operations (Op-413) Navy Department Washington 25, D. C.
1	Chief of Naval Operations (Op-20) Navy Department Washington 25, D. C.
1	Chief of Naval Operations (Op-32) Navy Department Washington 25, D. C.
6	Naval Research Laboratory (2000) Bellevue, D. C.
1	Naval Research Laboratory (2020) Bellevue D. C.
1	Naval Research Laboratory (3480) Bellevue D. C.
1	Naval Ordnance Laboratory White Oak Maryland

SS RP

-2-

- 1 U. S. Naval Electronics Laboratory
San Diego 52
California
- 1 Naval Air Development Center (AAEL)
Johnsville,
Pennsylvania
- 1 U. S. Navy Underwater Sound Laboratory
New London
Connecticut
- 1 U. S. Navy Office of Naval Research
Branch Office
150 Causeway Street
Boston 14, Massachusetts
- 1 U. S. Navy Office of Naval Research
Branch Office
346 Broadway
New York 13, N. Y.
- 1 U. S. Navy Office of Naval Research
Branch Office
The John Crerar Library Building
86 E. Randolph Street
Chicago 1, Illinois
- 1 U. S. Navy Office of Naval Research
Branch Office
801 Donahue Street
San Francisco 24, California
- 1 U. S. Navy Office of Naval Research
Branch Office
1030 Greene Street
Pasadena 1, California
- 2 U. S. Navy Office of Naval Research
U. S. Navy No. 100, Fleet Post Office
New York, N. Y.
- 1 Librarian
U. S. Naval Post Graduate School
Electronics Department
Monterey, California
- 1 U. S. Coast Guard(EEE)
1300 "E" Street, N. W.
Washington, D. C.

- 1 Research and Development Board
Pentagon Building
Washington 25, D. C.
- 1 Dr. N. Smith
National Bureau of Standards
Department of Commerce
Washington, D. C.
- 1 Applied Physics Laboratory
Johns Hopkins University
8621 Georgia Avenue
Silver Spring, Maryland
- 7 Library of Congress
Navy Research Section
Washington 25, D. C.
- 1 Dr. A. G. Hill
Project Lincoln
Massachusetts Institute of Technology
Cambridge 39, Massachusetts
- 1 Professor K. Spangenberg
Stanford University
Stanford, California
- 1 Professor E. C. Jordan
University of Illinois
Urbana, Illinois
- 1 Dr. V. H. Rumsey
Ohio State University
Columbus, Ohio
- 1 Dr. C. R. Burrows
Department of Electrical Engineering
Cornell University
Ithaca, New York
- 1 Electrical Engineering Department
University of California
Berkeley, California
- 1 Professor J. J. Brady
Oregon State College
Corvallis, Oregon
- 1 Electrical Engineering Department
University of Texas
Box F, University Station
Austin, Texas

- 1 Library
Philco Corporation
Philadelphia 34, Pennsylvania
- 1 Technical Library
Bell Telephone Laboratories, Inc.
Murray Hill, New Jersey
- 2 Librarian
National Bureau of Standards
Washington 25, D. C.
- 1 Librarian
Radio Corporation of America
RCA Laboratories Division
Princeton, New Jersey
- 1 Exchange Section, American and British
Exchange and Gift Division
Library of Congress
Washington 25, D. C.
- 1 Professor Morris Kline
Mathematics Research Group
New York University
45 Astor Place
New York, N. Y.
- 1 Technical Library
Federal Telecommunications
500 Washington Avenue
Nutley 10, New Jersey
- 1 Librarian
Central Radio Propagation Laboratory
National Bureau of Standards
Washington 25, D. C.
- 1 Mr. R. E. Campbell
Room 22-B-104
Massachusetts Institute of Technology
Cambridge 39, Massachusetts
- 1 Watson Laboratories Library, AMC
Red Bank
New Jersey
(ENAGSI)
- 1 Mr. J. Hewitt, Document Room
Research Laboratory of Electronics
Massachusetts Institute of Technology
Cambridge 39, Massachusetts

- 1 Dr. John V. N. Granger
Stanford Research Institute
Stanford, California
- 1 Radiation Laboratory
Johns Hopkins University
1315 St. Paul Street
Baltimore 2, Maryland
- 1 Mr. R. Damon
The Knolls
General Electric Company
Schenectady, N. Y.
- 1 Mrs. Mary Timmins, Librarian
Radio and Television Library
Sylvania Electric Products
70 Forsythe Street
Boston 15, Massachusetts
- 1 Library of the College of Engineering
University Heights Library
University Heights 53, New York
- 1 Documents and Research Information Center
Raytheon Manufacturing Company
Equipment Engineering Division
Newton, Massachusetts
- 1 Professor W. B. Davenport, Jr.
Lincoln Laboratory
Massachusetts Institute of Technology
Lexington, Massachusetts
- 50 Dr. H. A. Zahl
Transportation Officer
Second Avenue and Langford Street
Asbury Park, New Jersey
Contract N5ori-76, T. O. I.
- 50 Chief, Administration Section
Division Services Branch
Electronics Research Division
Air Force Cambridge Research Center
230 Albany Street
Cambridge 39, Massachusetts